

1 **Climate change increases riverine carbon outgassing while export to**
2 **the ocean remains uncertain**

3

4 F. Langerwisch^{1,2}, A. Walz³, A. Rammig^{1,4}, B. Tietjen^{5,2}, K. Thonicke^{1,2}, W. Cramer^{6,2}

5 ¹ Earth System Analysis, Potsdam Institute for Climate Impact Research (PIK), P.O. Box 60 12
6 03, Telegrafenbergs A62, D-14412 Potsdam, Germany

7 ² Berlin-Brandenburg Institute of Advanced Biodiversity Research (BBIB), 14195 Berlin,
8 Germany

9 ³ Institute of Earth and Environmental Science, University of Potsdam, Karl-Liebknecht-Str. 24-
10 25, D-14476 Potsdam-Golm, Germany

11 ⁴TUM School of Life Sciences Weihenstephan, Land Surface-Atmosphere Interactions,
12 Technical University Munich, Hans-Carl-von-Carlowitz-Platz 2, 85354 Freising, Germany

13 ⁵ Biodiversity – Ecological Modelling, Institute of Biology, Freie Universität Berlin,
14 Altensteinstr. 6, D-14195 Berlin, Germany

15 ⁶ Institut Méditerranéen de Biodiversité et d'Ecologie marine et continentale (IMBE), Aix
16 Marseille Université, CNRS, IRD, Avignon Université, Technopôle Arbois-Méditerranée, Bât.
17 Villemin - BP 80, F-13545 Aix-en-Provence cedex 04, France

18

19 *Correspondence to:* F. Langerwisch (langerwisch@pik-potsdam.de)

20

21 **Abstract**

22 Any regular interaction of land and river during flooding affects carbon pools within the
23 terrestrial system, riverine carbon, and carbon exported from the system. In the Amazon basin
24 carbon fluxes are considerably influenced by annual flooding during which terrigenous organic
25 material is imported to the river. The Amazon basin represents therefore an excellent example of
26 a tightly coupled terrestrial-riverine system. The processes of generation, conversion, and
27 transport of organic carbon in such a coupled terrigenous-riverine system strongly interact and
28 are climate-sensitive, yet their functioning is rarely considered in Earth system models and their
29 response to climate change is still largely unknown. To quantify regional and global carbon
30 budgets and climate change effects on carbon pools and carbon fluxes it is important to account
31 for the coupling between the land, the river, the ocean and the atmosphere. We developed the
32 riverine carbon model RivCM, which is directly coupled to the well-established dynamic
33 vegetation and hydrology model LPJmL in order to account for this large scale coupling. We
34 evaluate RivCM with observational data and show that some of the values are reproduced quite
35 well by the model while we see large deviations for other variables. This is mainly caused by
36 some simplifications we assumed. Our evaluation shows that it is possible to reproduce large
37 scale carbon transport across a river system however with large uncertainties. Acknowledging
38 these uncertainties, we estimate the potential changes in riverine carbon by applying RivCM for
39 climate forcing from five climate models and three CO₂ emission scenarios (SRES). We find that
40 climate change causes a doubling of riverine organic carbon in the Southern and Western basin
41 while reducing it by 20% in the Eastern and Northern parts. In contrast, the amount of riverine
42 inorganic carbon shows a 2- to 3-fold increase in the entire basin, independent of the SRES
43 scenario. The export of carbon to the atmosphere increases as well with an average of about
44 30%. In contrast, changes in future export of organic carbon to the Atlantic Ocean depend on the
45 SRES scenario and are projected to either decrease by about 8.9% (SRES A1B) or increase by
46 about 9.1% (SRES A2). Such changes in the terrigenous-riverine system could have local and
47 regional impacts on the carbon budget of the whole Amazon basin and parts of the Atlantic
48 Ocean. Changes in the riverine carbon could lead to a shift in the riverine nutrient supply and
49 pH, while changes in the exported carbon to the ocean leads to changes in the supply of organic
50 material that acts as a food source in the Atlantic. At larger scales the increased outgassing of
51 CO₂ could turn the Amazon basin from a sink of carbon to a considerable source. Therefore we
52 propose that the coupling of terrestrial and riverine carbon budget should be included in
53 subsequent analysis of the future regional carbon budget.

54

55 **1 Introduction**

56 Research on the effects of climate and land use change on terrestrial and riverine systems has
57 been extensively conducted. Results show how changes in temperature and precipitation will
58 affect the species composition in forest ecosystems (Fearnside, 2004; Huntingford et al., 2013;
59 Nepstad et al., 2007) as well as discharge and flooding patterns of rivers (Coe et al., 2011;
60 Panday et al., 2015; Zulkafli et al., 2016). However, the consequences for a coupled terrestrial-
61 riverine system have been elaborated on in less detail and mostly focusing on estimations under
62 the current climate (Johnson et al., 2006; Cole et al., 2000; Richey et al., 2002; Neu et al., 2011;
63 Abril et al., 2014). Here we want to deepen the understanding of consequences of climate change
64 on riverine carbon fluxes, which are fuelled by vegetation, and on the export of carbon from the
65 terrestrial part to the atmosphere and the ocean. We aim to understand how much the basin-wide
66 carbon balance is influenced by these interactions.

67 In this study we focus on the coupled terrestrial-riverine system on the Amazon basin. In this
68 region the Amazon River and in particular, the annually recurring flooding of parts of the forests,
69 shape the manifold Amazonian ecosystems. The flooding is most decisive for the coupling of
70 terrestrial and aquatic processes by transferring organic material from the terrestrial ecosystems
71 in the river (Hedges et al., 2000). The water rises with an amplitude of only some centimetres in
72 small tributaries to up to 15 meters in the main stem (Junk, 1985). In central Amazonia about
73 16% of the area is flooded during high water, while only 4% are flooded permanently (Richey et
74 al., 2002). During flooding, deposited litter and soil carbon which originates from terrestrial
75 vegetation is one source of organic material imported into the river system. The input of
76 terrigenous organic material affects the riverine system enormously on a local scale (Melack and
77 Forsberg, 2001; Waterloo et al., 2006). It acts, for instance, as fertilizer and food source
78 (Anderson et al., 2011; Horn et al., 2011), and is a modifier of habitats and interacting local
79 carbon cycles (Hedges et al., 2000; Irmler, 1982; Johnson et al., 2006; McClain and Elsenbeer,
80 2001). Whereas in most limnic systems additional organic material produced by aquatic
81 photosynthesis plays a major role for the riverine organic carbon pools (Lampert and Sommer,
82 1999; Schwoerbel and Brendelberger, 2005), the aquatic photosynthesis rate in large parts of the
83 Amazon River network is comparably low and submerged plants rarely occur (Junk and Piedade,
84 1997). Here, the input of allochthonous material produced in the floodplain forests is more
85 relevant than the production of organic matter within the river (Abril et al., 2014; Cole and
86 Caraco, 2001; Druffel et al., 2005; Mayorga et al., 2005). The low aquatic productivity in the
87 river system is caused by high sediment load and thus high turbidity in white water rivers and
88 low nutrient supply in the black water rivers (Benner et al., 1995; Richey et al., 1990; Sioli,
89 1957).

90 At larger scales, the release of carbon into the atmosphere and the export to the ocean are the
91 most relevant factors, when it comes to estimating the effects of Amazon ecosystems on climate
92 change. Approximately $32.7 \times 10^{12} \text{ g C yr}^{-1}$ (Moreira-Turcq et al., 2003) of total organic carbon

93 (TOC) is exported to the Atlantic Ocean, in comparison to about 470×10^{12} g C yr⁻¹ (Richey et
94 al., 2002) exported to the atmosphere as CO₂. While the carbon released to the atmosphere
95 proliferates climate change immediately, the carbon exported to the ocean affects the marine
96 ecosystems over hundreds of square kilometres off the mouth of the Amazon River, thereby
97 possibly influencing ocean-atmosphere carbon exchange over several weeks to months (Cooley
98 et al., 2007; Cooley and Yager, 2006; Körtzinger, 2003; Subramaniam et al., 2008).

99 Hydrologic or limnic production as well as transformation and export of carbon have been
100 estimated in a number of empirical (case) studies. These studies highlight different aspects of the
101 system, e.g. showing that the carbon within the river mainly originates from tree leaves and other
102 non-woody material from *Várzea* systems (Hedges et al., 2000; Moreira-Turcq et al., 2003),
103 describing reasons for temporal and spatial differentiations of organic matter within the river
104 (Aufdenkampe et al., 2007; Devol et al., 1995), and modelling the hydrological and biochemical
105 aquatic carbon budget over a 2000-km-reach (Bustillo et al. (2011)). Several studies already
106 combined the aquatic and the terrestrial compartment of the system by including the adjacent
107 forests (Johnson et al., 2006; Cole et al., 2000; Richey et al., 2002; Neu et al., 2011; Abril et al.,
108 2014), but these studies focus on estimating carbon budgets under current climate conditions.

109 By improving the understanding of how future climate change could influence the largest
110 interconnected ecosystem on Earth (Bauer et al., 2013; Sjögersten et al., 2014), an in-depth
111 analysis of the coupled terrigenous-riverine carbon fluxes and pools in the Amazon basin is
112 required. Climate and atmospheric CO₂, terrestrial productivity, water discharge and flooding
113 patterns strongly interact and thus control the amount of carbon in the Amazon river. But they
114 also influence its further conversion and transport within the river system, which finally
115 determine carbon export to either atmosphere or ocean. This tight coupling of the terrigenous-
116 riverine system makes the Amazon basin highly sensitive for climate change impacts.

117 This study aims at taking first steps towards an understanding of carbon fluxes in a terrigenous-
118 river-ocean system under future climate change by addressing the following research questions
119 for the example of the Amazon basin :

- 120 1) How will the highly interdependent and strongly climate-controlled carbon fluxes and
121 pools in the Amazon basin change during the 21st century?
- 122 2) Which regions in the Amazon basin are likely to be most strongly impacted by climate
123 change?
- 124 3) How does climate change alter the proportion of carbon immediately released to the
125 atmosphere vs. carbon exported to the ocean?
- 126 4) How relevant is the amount of riverine outgassed carbon for the basin-wide carbon
127 budget in a changing climate?

128 To address these questions we developed the **Riverine Carbon Model** (RivCM) and applied it to
129 the Amazon Basin. RivCM is directly coupled to the dynamic vegetation and hydrology model
130 LPJmL (Bondeau et al., 2007; Gerten et al., 2004; Rost et al., 2008; Sitch et al., 2003). The

131 riverine carbon model focuses on the export, transport and conversion of terrestrial fixed carbon.
132 Carbon pools and fluxes for the most important transport and transformation processes are
133 validated for current conditions based on observational data from the Amazon basin.

134 To investigate potential future changes in the different carbon fluxes and pools, the model was
135 forced by climate change scenarios that cover a large range of uncertainty in climate change
136 projections for the Amazon basin. Based on these simulations, we identify areas most heavily
137 affected by climate change. We estimated temporal changes in the different carbon fluxes and
138 pools, as well as the carbon released to the atmosphere and exported to the ocean. To
139 additionally assess the benefit of including inundated areas in the model, a full factorial
140 experiment was conducted. Herewith the study aims to develop a concept to assess changes in
141 coupled terrestrial-riverine systems, which is a prerequisite to better quantify regional and global
142 carbon budgets and consequences of climate change.

143

144 **2 Methods**

145 The **Riverine Carbon Model** (RivCM) is a grid-based model simulating riverine carbon
146 dynamics on monthly time steps. It is coupled to the process-based dynamic global vegetation
147 and hydrology model LPJmL (Bondeau et al., 2007; Gerten et al., 2004; Rost et al., 2008; Sitch
148 et al., 2003). RivCM is driven by current and future climate and atmospheric CO₂ data. An
149 overview about the interconnection between the models and scenarios is given in Fig. 1.

150 **2.1 Model descriptions**

151 **2.1.1 The dynamic global vegetation and hydrology model LPJmL**

152 The process-based dynamic global vegetation and hydrology model LPJmL (Bondeau et al.,
153 2007; Gerten et al., 2004; Rost et al., 2008; Sitch et al., 2003) calculates carbon and
154 corresponding water fluxes globally with a spatial resolution of 0.5 × 0.5 degree (lat/lon) and
155 daily time steps. For the simulation of potential natural vegetation and the main processes
156 controlling its dynamics, LPJmL uses climate data (temperature, precipitation and cloud cover),
157 atmospheric CO₂, and soil texture as input. The main processes are photosynthesis based on
158 Farquhar et al. (1980) and Collatz et al. (1992), auto- and heterotrophic respiration,
159 establishment, mortality and phenology. These processes lead to dynamic changes in carbon
160 stored in the vegetation, litter and soil. Simulated water fluxes include evaporation, soil moisture,
161 snowmelt, runoff, discharge, interception and transpiration. Globally, LPJmL calculates the
162 performance of nine plant functional types in each grid cell, each of these representing an
163 assortment of species classified as being functionally similar. In the Amazon basin, LPJmL
164 primarily simulates three of these plant functional types, representing tropical evergreen and

165 deciduous forest and C4 grasses. The monthly aggregated amounts of carbon stored in litter and
166 soil, as well as the grid-cell's amount of discharged and stored water are used as an input to
167 RivCM.

168 LPJmL has been shown to reproduce current patterns of biomass production, river discharge, and
169 carbon emission through fire, also including managed land (Biemans et al., 2009; Bondeau et al.,
170 2007; Cramer et al., 2001; Fader et al., 2010; Gerten et al., 2004, 2008; Poulter et al., 2009a;
171 Rost et al., 2008; Sitch et al., 2003; Thonicke et al., 2010; Wagner et al., 2003). The observed
172 patterns in water fluxes, such as soil moisture, evapotranspiration, and runoff, are comparable to
173 stand-alone global hydrological models (Wagner et al., 2003; Gerten et al., 2004; Gordon et al.,
174 2004; Gerten et al., 2008; Biemans et al., 2009). Several studies on Amazonia have been
175 conducted showing the effect of climate change on NPP (Poulter et al., 2009b), on carbon stocks
176 (Gumpenberger et al., 2010), on the risk for forest dieback (Rammig et al., 2010) and also on
177 riverine related changes such as inundation patterns (Langerwisch et al., 2013; Zulkafli et al.,
178 2016). The ability of the model to realistically reproduce both, terrestrial carbon and water fluxes
179 and pools, makes it an excellent tool to investigate the coupling of the terrestrial and riverine
180 carbon in the Amazon basin.

181 **2.1.2 The riverine carbon model RivCM**

182 RivCM is a process-based model which simulates the most important processes impacting
183 different riverine carbon pools, namely import, conversion and export (see overview in Fig. 2).
184 The model calculates the four major ecological processes related to the riverine carbon budget of
185 the Amazon River: mobilization of terrigenous organic material (litter and soil carbon),
186 (mechanical) decomposition of terrigenous organic material, (biochemical) respiration of
187 terrigenous organic material, and outgassing of CO₂ to the atmosphere. These processes directly
188 control the most relevant riverine carbon pools, specifically particulate organic carbon (POC),
189 dissolved organic carbon (DOC), and inorganic carbon (IC), as well as outgassed carbon
190 (representing CO₂), and exported riverine carbon to the ocean (POC, DOC and IC). Since
191 RivCM is developed to simulate the fate of terrigenous carbon, it neglects the autochthonous
192 production of organic material within the river. A description of the model including sensitivity
193 analysis and parameterization can be found in the following and in the Supplementary
194 Information (SI).

195 The Amazon River mobilizes large amounts of terrigenous organic material from seasonally
196 flooded forests (*Litc* and *Soilc* in Fig. 2), where dead leaves and twigs are exported to the river
197 (Irmler, 1982; Wantzen et al., 2008). Given the high productivity in Amazonian forests, this
198 mobilization considerably increases the amount of organic material in the water (Junk, 1985;
199 Cole and Caraco, 2001; Junk and Wantzen, 2004). Johnson et al. (2006) and Cole et al. (2000)
200 showed that terrestrially fixed carbon from the floodplain forests is the major source of respired
201 organic matter within the river and lakes. In RivCM the *mobilization* process is presented by a
202 function that calculates the amount of mobilized terrestrially fixed carbon in currently inundated

203 areas (*POC* and *DOC* in Fig. 2) depending on the amount of available exportable terrestrial
204 organic carbon from dead matter. The monthly inundated area is calculated using current
205 discharge and discharge from the reference period 1971-2000 and potentially floodable area
206 (Langerwisch et al., 2013).

207 Another source of organic matter for the river is, besides the import of terrigenous material, the
208 allochthonous production. In most limnic systems the production of organic material by
209 photosynthesis by aquatic plants plays a major role in the organic carbon pool (Lampert and
210 Sommer, 1999; Schwoerbel and Brendelberger, 2005). In Amazonia, however, the aquatic
211 photosynthesis rate in large parts of the Amazon River network is comparably low and
212 submerged plants rarely occur (Junk and Piedade, 1997) since the white water rivers contain
213 large amounts of sediments and are thus turbid and the black water rivers contain only little
214 nutrients (Benner et al., 1995; Richey et al., 1990; Sioli, 1957). Therefore, the input of
215 allochthonous material produced in floodplain forests contributes much stronger to total organic
216 matter within the river than the production by aquatic plants (Cole and Caraco, 2001; Junk, 1985;
217 Junk and Wantzen, 2004). Therefore, the Amazon river itself is considered rather a transport
218 agent than a producer of organic material (Junk and Wantzen, 2004). For these reasons the
219 calculation of riverine primary production, via aquatic photosynthesis, has been omitted in the
220 model calculations.

221 In the river, the imported organic matter is decomposed by manual breakup by either abiotic
222 decomposition like grinding or by biotic fragmentation by shredders such as Gammaridae, or fish
223 (Hedges et al., 1994; Martius, 1997; Melack and Forsberg, 2001). Moreover, *decomposition*
224 includes the leaching of coarse and fine material to form dissolved organic carbon (*DOC* in Fig.
225 2) (Lampert and Sommer, 1999). This enlarges the surface for colonization by fungi and bacteria
226 which are responsible for biochemical decomposition (*respiration*) (Martius, 1997; Wantzen et
227 al., 2008). During heterotrophic respiration, most of the ingested carbon is released as CO_2 to the
228 water body (*IC* in Fig. 2).

229 *Outgassing*, i.e. evasion of gases from the water body, occurs, when the concentration of a
230 specific gas in the water body exceeds its saturation concentration which depends on temperature
231 and partial pressure (Schwoerbel and Brendelberger, 2005). Due to high carbon input into the
232 Amazonian rivers, large amounts of CO_2 and CH_4 are produced and saturate the water (Mayorga
233 et al., 2005; Richey et al., 2002). The outgassing of CO_2 contributes more than 95% to the total
234 outgassed carbon (Belger et al., 2011; Melack et al., 2004; Richey et al., 2002). We therefore
235 considered only the outgassing of CO_2 in the model (CO_2 in Fig. 2).

236 An overview of model input, comprising static data (describing fixed site conditions), and
237 dynamic data, like climate, atmospheric CO_2 concentration, and terrigenous organic carbon, is
238 given in Table 1. Physical constants are listed in Table 2. The following sections describe the
239 input data, modelling approach of individual processes and the coupling to LPJmL.

240 **Input data and RivCM model initialization**

241 *River type* and *river order* (Fig. 3), as well as *river area* which represents about 25% of the
 242 potential floodable area (Langerwisch et al., 2013; Richey et al., 2002), prescribe the size and
 243 characteristics of the river stretch. The *river type* of each cell was defined by combining
 244 information published by Sioli (1957), Irion (1976), and Diegues (1994), and can be either white,
 245 black or clear water. The river colour depends on the amount of sediments and dissolved organic
 246 material in the water. It determines amongst others the pH and the temperature. For
 247 simplification, very small catchments (smaller than the simulated resolution) of deviating river
 248 types were neglected and the dominant river type was used. River order is represented by three
 249 classes and defined by total annual discharge (headwater: $< 8 \times 10^3 \text{ m}^3 \text{ yr}^{-1}$; middle reach: 8×10^3
 250 to $2 \times 10^5 \text{ m}^3 \text{ yr}^{-1}$; lower reach: $> 2 \times 10^5 \text{ m}^3 \text{ yr}^{-1}$). We chose these classes because of their
 251 different characteristics, as it is discussed in the River Continuum Concept (Vannote et al.,
 252 1980). Each grid cell that receives the routed water (*rout cell*) is determined by a digital
 253 elevation model (as also in Rost et al., 2008). The water is routed with a slope depending flow
 254 velocity $v [\text{m s}^{-1}]$ (Langerwisch et al., 2013), which results in a distance that is routed through
 255 per month of about 13 cells (in the largest part of the basin).

256 Data input from LPJmL to RivCM

257 Monthly discharge ($M_{dis} [\text{m}^3 \text{ s}^{-1}]$), amount of water ($M_{wat} [\text{m}^3]$), soil water content for two soil
 258 layers (M_{swc1} within the upper soil layer ($soildepth_1=200\text{cm}$) and M_{swc2} within the lower soil
 259 layer ($soildepth_2=300\text{cm}$) [%]) are provided by LPJmL. Additionally, annual litter carbon (AL_{itc}
 260 [g m^{-2}]) and soil carbon ($ASoilc [\text{g m}^{-2}]$) are provided by LPJmL (see also Figs. 1 and 2). The
 261 coupling is unidirectional. RivCM uses the LPJ output as input, but the processes calculated are
 262 only affecting the carbon pools and fluxes in RivCM. The carbon stored in litter and soil is
 263 calculated in LPJmL, while for simplification the reduction of litter due to the mobilization is not
 264 fed back to LPJmL.

265 Atmospheric CO_2 concentration ($atmCO_2 [\text{ppm}]$) and monthly temperature ($T [\text{ }^\circ\text{C}]$) prescribing
 266 abiotic atmospheric conditions are derived from the climate input data sets (see section 2.2).

267 Water temperature

268 Water temperature at time $t [\text{ }^\circ\text{C}]$ depends on air temperature (T_{air_t}) [$^\circ\text{C}$] and river colour, given
 269 by *river type*. In white and clear water rivers the temperature is below air temperature. The
 270 calculation of water temperature of these rivers is conducted according to Eq. (1) based on
 271 Bogan et al. (2003), with T_t calculated as

$$T_t = 0.6946 \times T_{air_t} + 5.19 \quad (1)$$

272 The temperature in black water rivers is close to air temperature.

273 Temperature response

274 The respiration reaction calculated in RivCM at time t is adjusted according to the water
275 temperature T_t by a coefficient for temperature response T_{response_t} (Eq. (2)) (Lampert and
276 Sommer, 1999). Additionally to the temperature response in water (and water saturated soil), a
277 temperature response for (unsaturated) soils was calculated with Eq. (3).

$$T_{\text{response}_t} = e^{308.56 \times (\frac{1}{56.02} - \frac{1}{T_t + 46.02})} \quad (2)$$

$$T_{\text{response}_d} = T_{\text{response}_t} \times \frac{1 - (e^{\frac{Mswc_1 \times \text{soildepth}_1 + Mswc_2 \times \text{soildepth}_2}{\text{soildepth}_1 + \text{soildepth}_2}})}{1 - (e^{-1})} \quad (3)$$

278 This is based on the empirical relationship of temperature response in soils (Lloyd and Taylor,
279 1994, also applied in LPJmL) which is valid for temperatures above -40°C .

280 **Initialization of litter and soil carbon**

281 As initialization for $Litc$ and $Soilc$ in the first simulated month, RivCM uses the litter and soil
282 carbon stocks ($ALitc$, $ASoilc$) from LPJmL. Analogue to LPJmL, a further division of $Soilc$ into a
283 fast respiring fraction (10% $Soilc_{\text{fast}}$) and a slow respiring fraction (90% $Soilc_{\text{slow}}$) was calculated.
284 Additionally, the annually produced litter prior respiration is used in RivCM. Since LPJmL does
285 not account for inundation, which changes respiration, the respiration of litter in (partly) water-
286 saturated soils is calculated within RivCM.

287 In general, in tropical forests litter falls continuously throughout the year (Müller-Hohenstein,
288 1981). In forests, where the flooding triggers litter fall, a peak of litter fall occurs during rising
289 and high water stage (Irmler, 1982). Because this is not accounted for in LPJmL (Sitch et al.,
290 2003), the annual un-respired litter carbon pool provided by LPJmL, $ALitc_{\text{unresp}}$ was
291 heterogeneously partitioned over 12 months to initialize the monthly litter amount ($Litc_{\text{unresp}}$) in
292 RivCM (Fig. 2, INPUT box). With Eq. (4) and Eq. (5) the maximum amount of carbon was
293 distributed to the month with high water and the minimum (at least 10% of annual litter) was
294 distributed to the month with low water. This depended on the distance between the current
295 month to the distance between the month with high water peak and the month with low water
296 peak ($dist_{highlow}$). With this approach we achieved a skewed distribution of litter carbon. The
297 factor for the monthly fraction ($fraction_{mt}$) was calculated with

$$fraction_{mt} = \cos\left(\frac{m_t}{dist_{highlow}} \times \pi\right) + (1.0 + litfrac_{min}) \quad (4)$$

298 if the current month number (m_t ; from 0-11) is smaller than the distance between high and low
299 water peak ($dist_{highlow}$), to distribute the maximum amount of carbon to the month with high
300 water, or with

$$fraction_{mt} = -\cos\left(\frac{m_t - dist_{highlow}}{12 - dist_{highlow}} \times \pi\right) + (1.0 + litfrac_{min}) \quad (5)$$

301 if the current month number (m_t ; from 0-11) is larger than the distance between high and low
 302 water peak ($dist_{highlow}$) to distribute the minimum amount of carbon ($\geq 10\%$ of annual litter) to
 303 the month with low water. Equation (4) calculates the convex part of the function, while Eq. (5)
 304 calculates the concave part of the function. The first part of both equations represents the cosine
 305 portion, and the second part sets the minimum of litter for the month with the low water peak
 306 $litfrac_{min}$.

307 By calculating the fraction of current monthly litter production versus total litter production in
 308 the course of each year (Eq. (6)), the total monthly un-respired litter carbon ($Litc_{unresp}$) can be
 309 determined with Eq. (7).

$$mfrac{t} = \frac{fraction_{m_t}}{\sum_{t=0}^{11} fraction_{m_t}} \quad (6)$$

$$Litc_{unresp_t} = mfrac{t} \times ALitc_{unresp} \quad (7)$$

310 **Respiration of litter and soil carbon**

311 The initialized litter and soil carbon pools ($Litc$, $Soilc$) are respiration and re-filled with the amount
 312 of the respiration of un-respired litter carbon ($Litc_{unresp}$). The calculation of respiration of organic
 313 matter depends on soil water content and temperature. The soil water content ($Mswc$) in un-
 314 inundated grid cells was provided by LPJmL, while the soil water content of (partly) inundated
 315 cells was calculated depending on the fraction of cell covered with water in RivCM. In inundated
 316 parts of the grid cell the soil water content was set to 100%. The respiration of the un-respired
 317 litter carbon and the soil carbon was calculated analogous to the LPJmL routine (for details see
 318 also SI Eqs. (S1) to (S12)) and is updated in each time step.

319 **Mobilization**

320 The mobilization function calculates the amount of mobilized terrestrially fixed carbon
 321 dependent on the amount of available exportable organic carbon on land, and on the size of
 322 inundated area. This area is determined using current discharge, reference discharge and
 323 potentially floodable area. The mobilization is not dependent on the river type, since the physical
 324 conditions of moving water to mobilize terrigenous material are the same on black and white
 325 water rivers.

326 Size of monthly inundated area

327 The inundated area at time t ($InunArea_t$ [km^2]) was defined as the area covered by water,
 328 including river and floodplain. It is determined by the current monthly discharge ($Mdis_t$ [$\text{m}^3 \text{s}^{-1}$])
 329 relative to the mean maximum discharge of the reference period 1971-2000 ($RefMeanMaxMdis$
 330 [$\text{m}^3 \text{s}^{-1}$]) produced under the climate forcing of CRU TS2.1 (Österle et al., 2003; Mitchell and
 331 Jones, 2005). The potentially floodable inundated area ($MaxInunArea$ [km^2]) Langerwisch et al.,

332 2013) (Eq. (8)) MaxInunArea [km^2] was calculated using the fraction of the cell that is potentially
 333 floodable (Langerwisch et al., 2013) multiplied by the cell area. The potentially floodable area
 334 was calculated by applying a modified Topographic Relative Moisture Index (based on Parker,
 335 1982) to a digital elevation model provided by the WWF database HydroSHEDS (WWF
 336 HydroSHEDS, 2007) as described by Langerwisch et al. (2013).

$$\text{InunArea}_t = \frac{\text{Mdis}_t}{\text{RefMeanMaxMdis}} \times \text{MaxInunArea} \quad (8)$$

337 If the current monthly discharge is very high and thereby larger than the mean maximum
 338 discharge of the reference period, the inundated area can exceed the potentially floodable area.

339 Because the export of terrigenous organic material is highest close to the river, each cell is
 340 subdivided into six sections, to account for spatial differentiation depending on the vicinity to the
 341 river. The size of the sections one to five is calculated with an exponential function (Eq. (9)). The
 342 remaining cell area is allocated to section six. The river area is assigned to the cell sections
 343 starting from the smallest section (Fig. S1). The river can expand into the next larger section
 344 during rising water. The largest section has the largest distance to the river and is therefore only
 345 occasionally inundated.

$$\text{size}_{\text{section}} = \frac{1}{e^{(\text{number}_{\text{section}}+1)}} \quad (9)$$

346

347 Size of floodplain area

348 The floodplain area (FloodplainArea [km^2]) at time t equals the inundated area that is not
 349 permanently covered with water. It was calculated by subtracting the river area (25% of
 350 inundated area, Richey et al., 2002) from the inundated area using Eq. (10) (see also
 351 Langerwisch et al., 2013).

$$\text{FloodplainArea}_t = \text{InunArea}_t - (0.25 \times \text{MaxInunArea}) \quad (10)$$

352 Amount of exported litter and soil carbon

353 This function calculates the amount of carbon exported from the terrestrial litter and soil pools to
 354 the river. River and forests at the headwater, which is defined by an annual discharge of less than
 355 $8 \times 10^3 \text{ m}^3 \text{ yr}^{-1}$ (river order 1 in Fig. 3B), are assumed to be much closer interconnected than at
 356 middle and lower reaches (order 2 and 3). Since small streams at the headwater directly flow
 357 beneath the trees, their export of litter and soil carbon was calculated from the entire inundated
 358 area. In all cells of higher river orders the export of terrestrial organic material occurs in the
 359 model only from the floodplain area and not from the permanently flooded river.

360 The *Igapó* forests which are inundated by black water rivers produce approximately 35% less
 361 litter and soil carbon (Worbes, 1997) compared to white water inundated *Várzea* forests. LPJmL

362 simulates tropical rainforest which is analogue to Várzea. Since LPJmL does not account for the
 363 different forest types, a correction of the organic material is performed for the Igapó forests.
 364 Hence, the amount of exportable organic material from the black water cells at time t is reduced
 365 by a factor of 0.35 (1–*carboncorr*; details in Table 3, Eqs. (11) and (12)).

$$Litc_{t_{corr}} = Litc_t \times carboncorr \quad (11)$$

$$Soilc_{t_{corr}} = Soilc_t \times carboncorr \quad (12)$$

366 For simplicity the following equations do only refer to *Litc*, instead of to the corrected value
 367 *Litc_{corr}* in case of *Igapó*.

368 The mobilization of litter and soil carbon at time t ($mLitc_t$, $mSoilc_t$, [10^6 g C cell $^{-1}$]) is calculated
 369 using the specific mobilization rates for litter and soil carbon (Table 3, Eqs. (13) and (14)).

$$mLitc_t = Litc_t \times FloodplainArea_t \times mobil_{litc} \quad (13)$$

$$mSoilc_t = Soilc_t \times FloodplainArea_t \times mobil_{soilc} \quad (14)$$

370 According to Irmler (1982), litter carbon is mobilized with a rate of 0.4 month $^{-1}$. After a
 371 sensitivity analysis this rate ($mobil_{litc}$) was calibrated to 0.7 month $^{-1}$ (see SI). Soil carbon
 372 mobilization takes place at a much smaller rate. Since no detailed value is available, the rate of
 373 soil mobilization ($mobil_{soilc}$) was calibrated after a sensitivity analysis to 0.05 month $^{-1}$. Mobilized
 374 carbon [10^6 g C cell $^{-1}$], originating from litter and soil, consists of a particulate ($mPOC_t$) and a
 375 dissolved ($mDOC_t$) carbon pool with the fractions of $mobil_p$ and ($1.0 - mobil_p$), respectively
 376 (Table 3, Eqs. (15) and (16)).

$$mPOC_t = (mLitc_t + mSoilc_t) \times mobil_p \quad (15)$$

$$mDOC_t = (mLitc_t + mSoilc_t) \times (1.0 - mobil_p) \quad (16)$$

377 The fraction of mobilized particulate carbon ($mobil_p$) was set to 0.5 according to McClain and
 378 Elsenbeer (2001) and Johnson et al. (2006) and was evaluated in a sensitivity analysis (SI).

379 Decomposition

380 Depending on the rate of decomposition ($decomp$ [month $^{-1}$], Table 3), the model calculates the
 381 conversion from particulate ($mPOC_t$) into dissolved organic carbon ($dDOC_{t+1}$) which has been
 382 estimated to be about 0.3 month $^{-1}$ by Furch and Junk (1997). In the calculations this rate was
 383 modified according to the river type. Along black water rivers the leaves are more sclerophyllous
 384 and thus much slower degradable (Furch and Junk, 1997). Therefore, the decomposition rate in
 385 black water cells is reduced by factor 0.9 (1.0 – *decompcorr*) based on Furch and Junk (1997)

386 (Table 3). The decomposed particulate organic carbon at time t $dPOC_t$ (Eq. (17)) was removed
 387 from the particulate organic carbon pool and added to the dissolved organic carbon pool
 388 (Eqs.(18) and (19)). The dissolved organic carbon is not fragmented any further.

$$dPOC_t = mPOC_t \times decomp \times decompcorr \quad (17)$$

$$dPOC_{t+1} = mPOC_t - dPOC_t \quad (18)$$

$$dDOC_{t+1} = mDOC_t + dPOC_t \quad (19)$$

389 Respiration

390 The respiration function calculates the decrease of particulate and dissolved organic carbon
 391 ($dPOC_{t+1}$, $dDOC_{t+1}$, [10^6 g C cell $^{-1}$]) by the respiration loss ($rPOC_{loss}$ and $rDOC_{loss}$) and the
 392 associated increase of dissolved inorganic carbon (rIC_{t+1}) at time t (Eqs. (20) to (24)). For this, a
 393 sufficient abundance of respiring organisms is assumed. In contrast to different decomposition
 394 rates in black and white water rivers, which is due to the fact that leaves at black water rivers
 395 tend to be more sclerophyllous and therefore less easily degradable, for the respiration of already
 396 degraded organic material we assume only minor differences. As soon as the leaves and twigs
 397 are degraded to small particles we assume that they react similarly. Therefore, respiration only
 398 depends on the rate of respiration loss ($respi$ [month $^{-1}$], see Table 3) and the temperature
 399 response ($Tresponse$, Eq. (2)).

$$rPOC_{loss} = dPOC_{t+1} \times (1 - e^{-(respi \times Tresponse_t)}) \quad (20)$$

$$rDOC_{loss} = dDOC_{t+1} \times (1 - e^{-(respi \times Tresponse_t)}) \quad (21)$$

$$rPOC_{t+1} = dPOC_{t+1} - rPOC_{loss} \quad (22)$$

$$rDOC_{t+1} = dDOC_{t+1} - rDOC_{loss} \quad (23)$$

$$rIC_{t+1} = IC_t + rPOC_{loss} + rDOC_{loss} \quad (24)$$

400 Outgassing

401 The model calculates the monthly saturation concentration of CO₂ $saturationC_t$ in the water
 402 $Mwat_t$ [m 3] (Eq. (25))

$$saturationC_t = k_H^\theta \times e^{d\ln k_H \times \left(\frac{1}{T_t + 273.15} - \frac{1}{T^\theta} \right)} \times \frac{atmCO_2 t}{10^6} \times ctoco2 \times Mwat_t \times 10^3 \quad (25)$$

403 using Henry's Law (Sander, 1999) and applying Henry's law constant (k_H^θ [g CO₂ l⁻¹ atm⁻¹])
 404 under standard conditions ($T^\theta = 298.15\text{K}$), temperature dependence of the Henry's law constant
 405 ($dlnkH$ [K]), the ratio of carbon to carbon dioxide ($ctoco2$), and monthly temperature T_t in °C.
 406 Depending on the river type, which determines the pH of the water, we calculated the amount of
 407 CO₂, HCO³⁻ and CO₃²⁻. For calculating the actual outgassing we only take the carbon into
 408 account, instead of the chemical form in which it exists. Afterwards, monthly saturation is
 409 multiplied with a monthly saturation factor ($co2satur$, Eq. (26), Table 3), which accounts for the
 410 super-saturation of the water with CO₂. These values depend on the hydrograph and were
 411 extracted from Richey et al. (2002). The difference between inorganic carbon amount and
 412 saturation concentration was added to the atmosphere carbon pool ($Icoutgast_{t+1}$, Eq. (27)), while
 413 carbon in the river equals the saturation concentration (oIC_{t+1} , Eq. (28)).

$$saturationCcorr_t = saturationC_t \times co2satur \quad (26)$$

$$Icoutgas_{t+1} = Icoutgas_t + (rIC_{t+1} - saturationCcorr_t) \quad (27)$$

$$oIC_{t+1} = saturationCcorr_t \quad (28)$$

414 2.2 Climate data sets

415 For model evaluation, climate forcing data from a homogenized and extended CRU TS2.1 global
 416 climate dataset (Österle et al., 2003; Mitchell and Jones, 2005) were used. Annual atmospheric
 417 CO₂ concentrations were prescribed as given by Keeling and Whorf (2003).

418 For the assessment of climate change impacts, three SRES scenarios (A1B, A2, B1)
 419 (Nakićenović et al., 2000) were applied. Five General Circulation Models (GCMs) (Jupp et al.,
 420 2010; see also Randall et al., 2007), namely, MIUB_ECHO_G, MPI_ECHAM5, MRI_CGCM2_3_2A,
 421 NCAR_CCSM3_0, UKMO_HADCM3 were chosen to cover a wide range of uncertainty within
 422 climatic projections with respect to precipitation patterns and temperature. The GCMs used the
 423 SRES scenarios to calculate future climate. For example, the model MIUB_ECHO_G shows a
 424 shortening of the dry season (defined by less than 100 mm precipitation per month), whereas
 425 UKMO_HADCM3 shows an elongation of the dry season towards the end of the century.
 426 Temperature in the Amazon basin is projected to increase under the A1B emission scenario by
 427 about 3.5K, by up to 4.5K for A2, and by up to 2 to 2.5K for B1 until the end of the century
 428 (Meehl et al., 2007). Projected rainfall differs considerably in spatial distribution within the
 429 Amazon basin among climate models. Under A1B, for instance, a decrease in precipitation is
 430 projected for Southern Amazonia (especially during the southern-hemisphere winter), whereas
 431 an increase in precipitation is projected in the Northern part (for details see Meehl et al., 2007).
 432 The projected climate data were bias-corrected with the CRU TS2.1 global climate dataset

433 (Österle et al., 2003; Mitchell and Jones, 2005). Annual future atmospheric CO₂ concentrations
434 are based on the respective SRES scenario.

435 All monthly climate data (observed and projected) were disaggregated to 'quasi-daily' values as
436 described by Gerten et al. (2004).

437 **2.3 RivCM calibration and evaluation**

438 To identify the most important explaining variables (parameters) and the most sensitive response
439 variables (carbon pools), a redundancy analysis (RDA) was performed. Based on the analysis we
440 calibrated *mobil_{litr}* and *mobil_{soilc}* (see SI).

441 To evaluate the performance of RivCM, a comparison of observed with simulated data was
442 conducted. TOC, POC, and DOC concentration were chosen, as well as exported carbon to the
443 ocean (TOC, POC, and DOC per year) and exported carbon to the atmosphere (outgassed CO₂
444 per year on different spatial domains) (see Table 4). The estimates of carbon exported to the
445 Atlantic Ocean are from the gauging station at Óbidos. The data from this station represent an
446 integration of information over the entire Amazon basin. Therefore they do not reflect large
447 temporal or spatial deviation over the basin and enable us to compare aggregated measured data
448 with aggregated simulated data. If possible, data from the same time period were compared. If
449 the observation period was after the last simulation year 2003, the data were compared to
450 simulated values from the reference period (1971-2000). The results of the evaluation can be
451 found in the SI.

452 **2.4 Modelling protocol and simulation experiments**

453 We performed LPJmL simulations with potential natural vegetation only, i.e. without land use,
454 on a 0.5° × 0.5° spatial resolution. To obtain equilibria for vegetation distribution, carbon and
455 water pools in LPJmL, all transient LPJmL runs were preceded by a 1000-years-spinup during
456 which the pre-industrial CO₂ level of 280 ppm and the climate of the years 1901-1930 were
457 repeated. All transient runs of the coupled model LPJmL-RivCM were preceded by a 90-years-
458 spinup during which the climate and CO₂ levels of 1901-1930 were repeated to obtain equilibria
459 for riverine carbon pools. Transient climate simulations are then performed for current climate
460 (1901-2003) and future climate (2004-2099). The data sets used are described in the section 2.2.

461 To identify how relevant the amount of riverine outgassed carbon for the basin-wide carbon
462 budget in a changing climate is, we compared the output of coupled-terrestrial-riverine
463 modelling runs with purely terrestrial or purely riverine modelling settings. The three different
464 factorial settings are the following:

465 Setting 1 (*Standard*) refers to the standard RivCM simulation including the actual river and the
466 additionally inundated area. In these simulations the export of organic material from the land

467 to the river was calculated, as well as the discharge of carbon to the ocean, aquatic outgassing
468 and release of CO₂ via terrestrial heterotrophic respiration.

469 Setting 2 (*NoInun*) includes the actual river, but excludes additional inundation. For this purpose,
470 the cell fraction, which is not permanently covered by water, remains dry to emulate no
471 coupling of land and river. In this simulation experiment no export of organic material from
472 the land to the river was calculated (i.e. there is no input of terrigenous organic material into
473 the river). Hence, no discharge of carbon to the ocean, no outgassing, but release of CO₂ from
474 the terrestrial heterotrophic respiration was calculated.

475 Setting 3 (*NoRiv*) includes calculations in which the original LPJmL results for CO₂ release from
476 vegetation only were used, i.e. the influence of the river and inundation were not accounted
477 for. In these simulations no outgassing from the water and no discharge of carbon to the ocean
478 was calculated. In contrast, outgassing from the heterotrophic respiration of the forest, also in
479 the areas in which RivCM simulates river area, was calculated.

480 In a full factorial design, all inundation scenarios (*Standard*, *NoInun* and *NoRiv*) were run for all
481 climate scenarios for future and current climate.

482 2.5 Analyses of future changes in the coupled terrigenous-riverine system

483 The effect of climate change is estimated by calculating the differences between carbon values in
484 a future period (2070-2099) and a reference period (1971-2000). Four different carbon pools
485 were analysed, namely outgassed carbon (atmospheric), riverine particulate organic carbon
486 (POC) and dissolved organic carbon (DOC), as well as the riverine inorganic carbon pool (IC)
487 and. The relative changes in POC and DOC are spatially and temporally similar (Fig. S4).
488 Therefore, only POC is shown and discussed in detail.

489 The spatial distribution of climate change effects (E_{CC}) on the different carbon pools and fluxes
490 (indicated by n) were estimated by calculating for each cell the quotient (Eq. (29)) of future values
491 (mean of 2070-2099) and reference values (mean of 1971-2000). To equalize a tenfold increase
492 (10^{+1}) and a reduction to one tenth (10^{-1}), the quotient was log-transformed (\log_{10}).

$$E_{CC_n} = \log_{10} \frac{\sum_{n=2070}^{2099} C_n}{\sum_{n=1971}^{2000} C_n} \quad (29)$$

493 To show model uncertainty that arises from differences in climate model projections an indicator
494 of the agreement between simulation results was calculated, it indicates a common significant
495 increase or decrease, respectively, of three, four or all five climate models. In addition, the
496 significance (p-value <0.05) of the difference between reference and future was assessed by a
497 Wilcoxon Rank-Sum Test (Bauer, 1972). This test can be used for datasets that are not normally
498 distributed and is therefore applicable to these data with high intra-annual fluctuations.

499 Additionally to the analysis of spatial patterns, an analysis of changes in mean carbon pools over
500 time was conducted. As above, changes were expressed as the logarithm of the quotient between
501 annual future values and mean reference values. In addition to these relative changes, the
502 absolute values in both periods were compared. The analysis was conducted both for the whole
503 Amazon basin and for three selected subregions. These three regions, indicated in Fig. 6A, were
504 identified according to future changes in inundation patterns, discussed in Langerwisch et al.
505 (2013). These areas include a region in the Western basin with projected increase in inundation
506 length and inundated area (R1), a region covering the Amazon main stem (R2) with intermediate
507 changes in inundation and a region with projected decrease in duration of inundation and
508 inundated area (R3). For details of the exact position of these regions see Table 5.

509 All statistical analyses were conducted using several packages in R. For the sensitivity analysis
510 the package 'vegan' (Oksanen et al., 2011) and for the analysis of the projections the packages
511 'stats' (R Development Core Team and contributors worldwide, 2011) and 'maptools' (Lewin-
512 Koh and Bivand, 2011) were used.

513

514 **3 Results**

515

516 **3.1 Validation of the simulation results**

517 To assess the potential changes of the riverine carbon pools and fluxes, it is essential that we
518 trust the model's ability reproduce observed patterns and fluxes. For this, the first step is to
519 validate river discharge before assessing carbon pools and fluxes. This has been done in
520 Langerwisch et al. (2013) for 44 gauging stations in the Amazon basin, and shows that the
521 observed discharge patterns can be reproduced. Here, we validated the carbon concentration and
522 export fluxes with published data (Table 4). If possible we compared the simulated with
523 observed values from the same period of time. We only included spatial data for which we could
524 find the exact location (longitude/latitude).

525 The validation of exported data shows that the outgassed carbon (export to the atmosphere) is
526 underestimated by the model on a small scale by more than 90% and on the basin wide scale by
527 70%. In contrast the organic carbon exported to the ocean is overestimated by the model by 70%.
528 However, on a sub-catchment level the overestimation of exported organic carbon is much
529 smaller. Comparing observed and simulated concentrations of POC, DOC and IC shows that
530 simulation results are within the observed range. For POC the simulated concentration is about
531 50% larger than the observed concentration, but with a range between -90% and +200%. For the

532 simulated DOC concentration the range is between -90% and +90%, while for IC the range is
533 between -70% and +60%.

534

535 **3.2 Changes in riverine carbon under future climate projections**

536 The amount of outgassed carbon (Fig 4A) is simulated to remain constant compared to 1971-
537 2000 until about 2020. This is followed by a clear increase. This increase is strongest in in region
538 R1 (mean +70%) while it is moderate in R2 and R3 (+30% and +20%, respectively). Generally,
539 the simulated increase is largest for the SRES A2 scenario, followed by the A1B and the B1
540 scenario (see also Fig. 5). The spread of simulated outgassed carbon is comparably large between
541 the five climate models. Outgassed carbon shows a basin wide increase (Fig. 6G-I). In most parts
542 of the basin the outgassed carbon increases only slightly but significantly ($p<0.05$; up to 2-fold).
543 In parts of the Andes the increase is up to 5-fold, shown by at least four of the five climate
544 models (as indicated by crosses in Fig. 6). In a few areas in the Southern Andes the outgassed
545 carbon decreases (0.3-fold).

546 The changes in POC (Fig. 4B) show a slight basin wide increase of about +10% (SRES mean)
547 until the end of the century. In region R1 this increase is larger, with +50% (SRES A2) and
548 +35% (SRES B1). In the regions R2 and R3 the POC amounts remain nearly constant (+5% and
549 ±0%, respectively). A wide range of possible paths of simulated POC amounts is spanned by the
550 five climate models, whereas the three emission scenarios only result in minor differences in
551 simulation results (see also Fig. 5). The spatial changes for POC show an up to 2-fold increase in
552 the Western and South-Western part of Amazonia for all three SRES emissions scenarios (Fig.
553 6A-C) with high agreement between the five climate models compared to the reference period.
554 In contrast, climate model agreement in the Northern and North-Western basin is lower and
555 shows a decreasing trend in the POC pool with a factor of 0.5. For the central part of the basin,
556 no clear trend is visible. POC seems to be less sensitive to different changes in atmospheric CO₂
557 concentrations compared to IC as only small regional differences were simulated with POC
558 increasing in the Western part of the basin under the A2 scenarios and decreasing in the Northern
559 part of the basin under the A1B scenario.

560 In contrast to outgassed carbon and DOC, riverine inorganic carbon (IC) increases basin wide
561 (Figs. 4C and 5) during the entire 21st century. Here, clear differences in the SRES emission
562 scenarios are found. In the SRES A2 scenario the increase is largest, with a basin wide increase
563 by +150% (+220% in R1, +150% in R2, and +140% in R3). In the B1 scenario the average
564 increase is smallest, with basin wide +50% (+80% in R1, +60% in R2, and +50% in R3). The
565 spatial distribution of changes in riverine inorganic carbon (IC, Fig. 6D-F) shows an overall
566 increase compared to the reference period. For at least four climate models this increase in IC is
567 significant ($p<0.05$), especially in the Western part of the basin. Here, the largest changes are
568 found for the SRES emission scenario A2 (up to 5-fold increase).

569 **3.3 Changes in the export of riverine carbon to ocean and atmosphere under**
570 **future climate**

571 Riverine outgassed carbon makes up on average 10% of total outgassed carbon along the river
572 network during the reference period (Fig. 8A). Total outgassed carbon includes carbon evaded
573 from the river and the forest. The carbon evaded from the forest reflects the amount of terrestrial
574 respiration (autotrophic and heterotrophic respiration). The average changes in this
575 proportion caused by climate change and the agreement of climate models (indicated by crosses)
576 on the direction of change are depicted in the three maps in Fig. 8B-D. The largest differences
577 are found under the SRES A2 scenario with the largest area in agreement between the climate
578 models (Fig. 8C). Here an increase of up to 7% in the proportion is found in the Western and
579 South-Western part of the Amazon basin. This increase is less pronounced in the other two
580 emission scenarios (Figs. 8B and 8D). For all SRES scenarios a slight decrease in the proportion
581 of up to 2% (-0.02) can be seen in parts of the North-Western basin and scattered in the very
582 South (Fig. 8B-D), this occurs because rivers will contribute increasingly to respiration losses of
583 carbon.

584 To estimate the relevance of riverine carbon to imported atmospheric carbon (via terrestrial
585 photosynthesis) or exported carbon (via outgassing or discharge to the ocean), results of the
586 factorial experiments were compared (Wilcoxon Rank-Sum Test; $p<0.001$, Table 6, see also
587 section 2.4). The standard RivCM results (*Standard*) were analysed to estimate the role of
588 riverine carbon to total carbon export. The simulated mean annual total organic carbon (TOC)
589 discharged to the ocean during the reference period (1971-2000) is about $54 \times 10^{12} \text{ g yr}^{-1}$ (Table
590 6). This represents approximately 1.0% of the basin net primary production (NPP). The export of
591 TOC to the ocean changes under climate change depends on the three SRES emission scenarios.
592 In the A1B scenario mean annual export decreases significantly by about 8.9% for 2070-2099
593 (compared to the reference period) for all five climate models, whereas under the A2 scenario the
594 TOC export increases by about +9.1%. The B1 scenario shows an intermediate change, with an
595 increase of about +4.6%. Depending on the emission scenario, the export of TOC to the ocean
596 decreases from about 1% of the NPP to about 0.75-0.9% of the NPP in the future period.

597 **3.4 Summary of overall changes in the carbon fluxes under climate change**

598 The first three research questions we addressed in this study were answered with the above
599 mentioned results. As a summary Fig 7 provides an aggregated picture of projected changes in
600 terrestrial carbon pools and resulting changes in riverine carbon pools. The moderate increase in
601 terrestrial carbon (on average +12.7% in biomass, +13.8% in litter carbon and +4.1% in soil
602 carbon) leads to a moderate increase of riverine organic carbon (POC +10.7% and DOC +8.3%),
603 but due to an increased CO_2 partial pressure the outgassed carbon increases by about 42.6%,
604 whereas the discharged carbon increases only by about 1.1%.

605

606 **3.5 Relevance of the riverine outgassed carbon**

607 To assess the relevance of riverine carbon for total carbon export to the atmosphere, either from
608 the forest (heterotrophic respiration) or from the water, the standard RivCM results (*Standard*)
609 were compared to results of the *NoInun* experiment and the *NoRiv* experiment (Table 6). In the
610 reference period the total outgassed carbon is estimated to be about 440×10^{12} g month⁻¹,
611 calculated in the standard RivCM simulations (*Standard*). Under climate change this amount
612 increases by 23%, 28%, and 21% for emission scenarios A1B, A2 and B1, respectively. The
613 proportion of outgassed carbon from the river to total outgassed carbon is about 3.6% in the
614 reference period. This proportion increases in all emission scenarios to up to 3.9% to 4.3%.
615 During the reference period the amount of riverine outgassed carbon makes up about 3.5% of the
616 net primary production (NPP). In the future this proportion increases significantly to up to
617 4.25%.

618 The simulations without input of terrigenous organic material to the river, caused by suppressed
619 inundation (*NoInun*), lead to a reduction of total outgassed carbon. During the reference period it
620 is significantly reduced by about -3.30%. During the future period this reduction remains
621 relatively constant for all SRES scenarios. If the river area is substituted by potential forest cover
622 (*NoRiv*), the total terrestrial outgassed carbon is about 0.1% lower than the sum of terrestrial and
623 riverine outgassed carbon in the standard simulations. This proportion decreases slightly to 0.07-
624 0.10% in the future period.

625

626 **4 Discussion**

627 The main goal of our study was to develop a coupled terrestrial-riverine model for assessing
628 regional and global carbon budget, considering riverine carbon pools and fluxes and their
629 potential changes under climate change. We used the Amazon basin as a case study because it
630 represents a tightly coupled terrestrial-riverine system. To achieve our goal we combined the
631 newly developed riverine carbon model RivCM with the terrestrial vegetation model LPJmL. In
632 the following we discuss the performance of and uncertainties in the coupled model system, as
633 well as the mechanisms leading to projected changes in riverine carbon. Finally, we elaborate on
634 the importance of incorporating the terrestrial-riverine coupling in models to better understand
635 processes in terrestrial-riverine systems.

636 **4.1 Riverine carbon pools**

637 The model RivCM calculates the dynamics of several organic carbon pools and fluxes the
638 Amazon basin. A comparison of these carbon pools and fluxes with observation shows in
639 summary that model results are within the range of observed concentrations of both organic and
640 inorganic carbon pools, but the model underestimates the outgassed carbon strongly while it
641 overestimates the carbon discharged to the ocean.

642 For the concentration of carbon the range of observations is large, mainly caused by the different
643 characteristics of the sub-catchments. The concentration of organic and inorganic carbon is
644 overestimated by the model for some sub-catchments, while it is underestimated for others. The
645 sub-catchments differ in their specific characteristics, such as water, soil and vegetation. The
646 model has difficulties to capture these differences. Including more side specific information for
647 the water, the vegetation and the characteristics of the river stretch could lead to a better match
648 between observation and simulation. However, the standard deviation of the observation is large
649 and for most of the cases the simulated concentration lies within the observed range. The
650 mismatch between the observation and the simulation might also be caused by an over or
651 underestimation of carbon exported to the river, which depends on the inundated area. The model
652 takes the nonlinear change in inundated area during flooding only simplified into account, which
653 might lead to an underestimation of flooded area. The relatively coarse spatial resolution might
654 also be a reason for the underestimation of the flooded area. The fixed ratio of 25% of the
655 potentially floodable area representing the river, might be less applicable to areas in the
656 headwater. We compared the fixed ration of 25% against observation in the lowlands (e.g.
657 Lauerwald et al., 2015; Lehner and Döll, 2004; Richey et al., 1990) and think that this ratio is
658 reasonable for the Amazon lowland. However, misestimating the actual floodplain river might
659 also lead to poor estimates of exported organic carbon. An additional cause of differences
660 between observed and simulated (inorganic) carbon amount might be that the model does not
661 take weathering, other carbon sources than terrigenous carbon, or the longer residence time of
662 water in the flooded forests into account. In summary the main reasons for the mismatch between
663 observations and simulations is due to some simplifications (spatially and within the processes)
664 we applied.

665 For the comparison of exported carbon to either the ocean or the atmosphere the model tends to
666 overestimate the discharge to the ocean, while it underestimates the outgassing. The amount of
667 discharged carbon is tightly coupled to the concentration and the water discharge. While the
668 discharge of water has been shown to be realistic (Langerwisch et al., 2013), and the simulated
669 concentration is within the observed range, a slight shift in the hydrograph can lead to the
670 mismatch between observed and simulated amount of exported carbon to the ocean. In addition,
671 the model might overestimate carbon exported to the ocean because it does not include dams.
672 These artificial structures can lead to a prolonged residence time of water and its transported
673 material, and thus to prolonged decomposition and an increased sedimentation (Goulding et al.,

674 2003). In the natural parts, such as floodplains, sedimentation especially impacts on the river bed
675 structure (Allison et al., 1995; Junk and Piedade, 1997). However, the sedimentation of organic
676 material is comparably small with only 50 g C yr^{-1} per square meter of water area (Melack et al.,
677 2009). Sedimentation and resuspension act on the small to medium scale (Junk and Piedade,
678 1997; Yarnell et al., 2006). On the spatial resolution of 0.5 degree both processes are assumed to
679 be balanced for organic carbon and have therefore not been explicitly calculated in the model,
680 but might be of importance at smaller scales. The amount of outgassed carbon from the water
681 body of the river to the atmosphere is probably underestimated because the way RivCM
682 calculates the inundated area and therewith the area of evasion does not include the cross-section
683 of the riverbed. Therewith the non-linear increase of inundated area with an increase in water
684 amount is not included. Including this would potentially lead to a larger inundated area, which
685 would increase the outgassing. The temporal resolution of monthly time steps might also be a
686 reason for the underestimation of the outgassing, because the time steps on which the outgassing
687 is calculated do not include permanent exchange with the atmosphere. The saturation
688 concentration is only updated monthly. An adjustment on shorter time steps could lead to a
689 higher outgassing.

690 For assessing the effects of climate change on riverine carbon and exported carbon pools and
691 fluxes, we calculated their relative differences. Although the absolute simulated amounts and
692 concentrations might not completely fit the observations, we are sure that the relative changes
693 still provide insights into potential future changes.

694 The riverine carbon pools and fluxes in this tightly coupled system may change during the 21st
695 century in several ways. According to our results climate change will induce a basin wide
696 increase in riverine carbon pools. Areas most affected are the central and western basin. Here the
697 outgassing of CO₂, as well as the organic and inorganic carbon pools increases most clearly.

698 Our results indicate that projected climate change may alter outgassed carbon (CO₂ evasion) by
699 several means. Firstly, a higher production of terrestrial material leads to an increase of organic
700 carbon available for respiration; secondly, the higher atmospheric CO₂ concentration leads to an
701 increase in dissolved inorganic carbon in the water. Thirdly, higher water temperatures decrease
702 the solubility of CO₂ in the water, but also increase the respiration rates. Overall a combination
703 of these factors may lead to a considerable increase in CO₂ evasion and a slight increase of
704 exported riverine carbon. Spatially the results are heterogeneous. The amount of outgassed
705 carbon increases in most parts of the basin. This pattern is mainly driven by the increased
706 amount of organic carbon available for respiration. However, even in areas where organic carbon
707 does not increase, or even decreases, the amount of outgassed carbon is elevated. This is mainly
708 caused by the increased respiration rate at higher temperatures. Thus, even with less carbon
709 available, higher temperatures lead to an elevated outgassing of CO₂. As a consequence of an
710 increased evasion of CO₂, an additional increase in atmospheric CO₂ concentration can occur.
711 However, the simulated amount of outgassed carbon under current conditions is underestimated

712 in comparison to observations by a factor of up to 1/6. The observations are based on a
713 combination of small scale measurements of CO₂ evasion and remotely sensed estimates of
714 inundated area (Belger et al., 2011; Moreira-Turcq et al., 2003; Richey et al., 1990, 2002). In
715 contrast, the outgassing calculated in RivCM is a more aggregated estimate. In reality during
716 rising water stage, small changes in discharge can lead to a comparably larger non-linear
717 increase in inundated area. This is not taken into account in RivCM. In RivCM the outgassing
718 depends only on the inorganic carbon concentration in the water and the partial pressure of CO₂.
719 Additionally to the inundated area, also the vegetation coverage affects the outgassing of CO₂
720 from flooded area as Abril et al. (2014) show. Including the production of allochthonous organic
721 material, which is not included in RivCM, might also change the amount of outgassed carbon.
722 But in contrast to the other processes the production via photosynthesis might lead to an increase
723 of the CO₂ evaded to the atmosphere. Furthermore, including the evasion of CO₂ from inundated
724 soils, which represents a process that might lead to a further increase of simulated CO₂
725 outgassing, into RivCM would help to simulate outgassing that is more in agreement with
726 observed estimates.

727 Besides riverine carbon fluxes such as outgassed carbon, climate change also affects riverine
728 carbon pools. However, these changes are not homogeneously distributed across the basin. The
729 increase in organic carbon (POC and DOC) is on one hand caused by the change in inundation
730 patterns. This can be seen mainly in the Western part of the basin, resulting from an projected
731 increase in precipitation, particularly in the SRES-A2 scenario (Langerwisch et al., 2013). On the
732 other hand, more rainfall and increased atmospheric CO₂ concentration may lead to increased
733 amounts of available organic carbon, i.e. more biomass under future climate conditions (e.g.
734 Huntingford et al., 2013), which may directly increase the POC and DOC pools. As a
735 consequence of the additional riverine organic carbon, a depletion of oxygen caused by enhanced
736 respiration in the water can occur (Junk and Wantzen, 2004; Melack and Fisher, 1983). The
737 resulting anoxia can lead e.g. to denitrification or production of methane (Lampert and Sommer,
738 1999). In areas with already reduced O₂ levels, such as flooded forests during falling water, the
739 further depletion of oxygen can potentially affect fish and other animal groups inhabiting the
740 water (Hamilton et al., 1997; Melack and Fisher, 1983). The comparison with measured data
741 (Cole and Caraco, 2001; Ertel et al., 1986; Hedges et al., 1994; Moreira-Turcq et al., 2003; Neu
742 et al., 2011) shows that the concentrations of the different simulated carbon pools fit in the range
743 of observations, with only a slight overestimation for POC. These results also show that the
744 inclusion of allochthonous organic material is not necessarily needed to reproduce the observed
745 POC concentrations in the water. The agreement of simulated with observed POC, DOC and IC
746 concentrations shows the reliability of RivCM, because the errors in concentration measurements
747 are small.

748 The amount of riverine inorganic carbon which remains in the water and does not evade to the
749 atmosphere is projected to increase under climate change. Here, the lower solubility resulting
750 from higher temperatures is not able to balance the effect of a higher atmospheric CO₂

751 concentration resulting in more dissolved CO₂. This pattern is consistent within the emission
752 scenarios and the climate models and can be found in most parts of the basin. The two- to
753 threefold increase in inorganic carbon in the water might have serious consequences for fish and
754 fungi, since dissolved inorganic carbon directly lowers the pH in the water (Lampert and
755 Sommer, 1999). In combination with the oxygen depletion discussed above this might severely
756 affect riverine fauna.

757 4.2 Riverine outgassing and export to the Atlantic Ocean

758 Our results indicate that climate change alters the proportion of carbon evaded from the river to
759 carbon exported to the ocean. Climate change increases the outgassing of CO₂ with a higher rate
760 than it increases the discharge of organic carbon.

761 During the reference period, the outgassed carbon from water bodies contributes on average
762 about 3.6% of all evaded carbon from the entire Amazon basin. This seems to be only a small
763 amount, but in river-dominated regions, this fraction may represent up to 10-50% of total evaded
764 carbon, which is especially obvious in the Eastern part of the basin. The basin-wide proportion of
765 riverine vs. total carbon evasion (including riverine outgassing and CO₂ release during
766 autotrophic and heterotrophic respiration) increases from 3.6% to up to 4.3% from the reference
767 to the future period, which indicates the increasing contribution of riverine outgassed carbon to
768 the total outgassed carbon. Our results show that 3.5% of the carbon accumulated in terrestrial
769 NPP is released to the atmosphere by outgassing from the river. It can be expected that climate
770 change will alter this fraction to up to 4.2% which is caused by a combination of increased NPP
771 and increased CO₂ partial pressure. Inland waters receive about 19×10^{14} g C yr⁻¹ from the
772 terrestrial landscape, of which about 8×10^{14} g C yr⁻¹ are returned to the atmosphere (Cole et al.,
773 2007). Globally the riverine input from land to ocean of organic carbon is estimated to be
774 between 4.5×10^{14} g C yr⁻¹ and 9.0×10^{14} g C yr⁻¹, which is at least the same amount of carbon that
775 is taken up by the oceans from the atmosphere (Bauer et al., 2013; Cole et al., 2007).

776 The annual export of freshwater from the Amazon river of about 6,300 km³ to the Atlantic Ocean
777 (Gaillardet et al., 1997) is accompanied by 40×10^{12} g of organic carbon, which represents 8-10%
778 of the global organic carbon transported to oceans by rivers (Moreira-Turcq et al., 2003; Richey
779 et al., 1990). Our estimates of the discharge of organic carbon to the Atlantic are larger. As
780 already shown in other studies (Gerten et al., 2004; Langerwisch et al., 2013) LPJmL is able to
781 reproduce observed discharge patterns. As already discussed (4.1.) small deviations between
782 observed and simulated discharge or even a small shift in seasonality (1-2 months) can lead to a
783 comparably large difference in discharged carbon, because the combination of the simulated
784 concentration and amount of water discharged determines the amount of discharged carbon to
785 the Atlantic Ocean. In addition to that, the overestimation of export to the ocean is partly caused
786 by up and downscaling of observation data. Our estimates of riverine TOC export represents
787 about 1-2% of the net basin primary production (Moreira-Turcq et al., 2003) is in agreement with

788 the results of our study (1% during reference period). Our results suggest that this proportion will
789 change by -10% to $+10\%$ due to climate change. The continuous input of organic matter into the
790 ocean fundamentally impacts the primary production of the Atlantic Ocean off the coast of South
791 America (Körtzinger, 2003; Cooley and Yager, 2006; Cooley et al., 2007; Subramaniam et al.,
792 2008). In addition to organic carbon, also nutrients, which are only marginally taken up by the
793 low primary production within the river, are exported to the ocean fuelling oceanic heterotrophy
794 and primary production, respectively.

795 The inclusion of inundation and the corresponding transport and conversion of organic material
796 leads to an increase in outgassed carbon of more than 3%, which equals to about
797 14.5×10^{12} g month $^{-1}$. This amount increases to up to 18.3×10^{12} g month $^{-1}$ due to climate change.
798 The proportion of outgassed carbon from water bodies is an indicator for the importance of the
799 riverine system to carbon dynamics of the entire basin. It emphasizes the importance of the
800 implementation of floodplain systems to vegetation models, especially for Amazonia. Including
801 inundation and export of organic material to vegetation models seems to be of minor importance,
802 because the carbon is only transported but its quantity does not change. This is only partly true
803 since the organic material is no longer available on site (e.g. as fertilizer) but is removed from
804 one location and finally from the entire system. Including this export leads to a more realistic
805 estimation of carbon fluxes, and ignoring this constant drain of carbon from the Amazon basin,
806 would therefore overestimate the general ability of Amazonia to sequester carbon. Only coupled
807 models can cover the interconnection between land and river, which might be important to
808 identify non-linear feedbacks on climate change (Bauer et al., 2013). Our approach serves as a
809 basis for simulating carbon modification and transport from the terrestrial biosphere through
810 river systems to the oceans and establishes the link between continental and oceanic systems on a
811 continental scale.

812 5 Summary

813 We aimed to develop a coupled terrestrial-riverine model to understand the effects of climate
814 change on carbon fluxes in such a coupled system. We applied the model to the Amazon basin
815 which could serve as a blueprint for studying other systems where such a tight coupling of the
816 terrestrial and riverine part appears. With our approach we were able to estimate potential
817 changes in exported and riverine carbon pools and fluxes from present until 2100 for the
818 Amazon basin. We showed that the export of carbon to the Atlantic Ocean could increase
819 slightly by about 1%, while the export to the atmosphere could increase by about 40%. To
820 estimate these changes we coupled the newly developed riverine carbon model RivCM to the
821 well-established vegetation and hydrology model LPJmL. These large export fluxes are
822 accompanied with changes in terrestrial organic carbon and riverine organic and inorganic
823 carbon. Our results suggest that coupling terrestrial with riverine carbon is an important step

824 towards a better understanding of the effects of climate change on large scale catchment carbon
825 dynamics.

826

827 *Author contributions.* Model development: FL, BT, WC. Data analysis: FL, AR, KT. Writing the
828 article: FL, AR, AW, BT, KT.

829 *Acknowledgements.* We thank “Pakt für Forschung der Leibniz-Gemeinschaft” for funding the
830 TRACES project for FL. AR was funded by FP7 AMAZALERT (ProjectID 282664) and
831 Helmholtz Alliance ‘Remote Sensing and Earth System Dynamics’. We also thank Susanne
832 Rolinski and Dieter Gerten for discussing the hydrological aspects. We thank Alice Boit for
833 fruitful comments on the manuscript. Additionally we thank our LPJmL and ECOSTAB
834 colleagues at PIK for fruitful comments on the design of the study and the manuscript. We also
835 thank the reviewers whose comments and suggestions largely improved the manuscript.

836

837 **6 References**

838 Abril, G., Martinez, J.-M., Artigas, L. F., Moreira-Turcq, P., Benedetti, M. F., Vidal, L.,
839 Meziane, T., Kim, J.-H., Bernardes, M. C., Savoye, N., Deborde, J., Souza, E. L., Albéric, P.,
840 Landim de Souza, M. F. and Roland, F.: Amazon River carbon dioxide outgassing fuelled by
841 wetlands, *Nature*, 505(7483), 395–398, doi:10.1038/nature12797, 2014.

842 Allison, M. A., Nittrouer, C. A. and Kineke, G. C.: Seasonal sediment storage on mudflats
843 adjacent to the Amazon river, *Mar. Geol.*, 125(3-4), 303–328, 1995.

844 Anderson, J. T., Nuttle, T., Saldaña Rojas, J. S., Pendergast, T. H. and Flecker, A. S.: Extremely
845 long-distance seed dispersal by an overfished Amazonian frugivore, *Proc. R. Soc. B Biol. Sci.*,
846 278, 3329–3335, doi:10.1098/rspb.2011.0155, 2011.

847 Aufdenkampe, A. K., Mayorga, E., Hedges, J. I., Llerena, C., Quay, P. D., Gudeman, J.,
848 Krusche, A. V. and Richey, J. E.: Organic matter in the Peruvian headwaters of the Amazon:
849 Compositional evolution from the Andes to the lowland Amazon mainstem, *Org. Geochem.*,
850 38(3), 337–364, doi:10.1016/j.orggeochem.2006.06.003, 2007.

851 Bauer, D. F.: Constructing confidence sets using rank statistics, *J. Am. Stat. Assoc.*, 67(339),
852 687–690, 1972.

853 Bauer, J. E., Cai, W.-J., Raymond, P. A., Bianchi, T. S., Hopkinson, C. S. and Regnier, P. A. G.:
854 The changing carbon cycle of the coastal ocean, *Nature*, 504(7478), 61–70,
855 doi:10.1038/nature12857, 2013.

- 856 Belger, L., Forsberg, B. R. and Melack, J. M.: Carbon dioxide and methane emissions from
857 interfluvial wetlands in the upper Negro River basin, Brazil, *Biogeochemistry*, 105, 171–183,
858 doi:10.1007/s10533-010-9536-0, 2011.
- 859 Benner, R., Opsahl, S., Chin-Leo, G., Richey, J. E. and Forsberg, B. R.: Bacterial carbon
860 metabolism in the Amazon River system, *Limnol. Oceanogr.*, 40(7), 1262–1270, 1995.
- 861 Biemans, H., Hutjes, R. W. A., Kabat, P., Strengers, B. J., Gerten, D. and Rost, S.: Effects of
862 precipitation uncertainty on discharge calculations for main river basins, *J. Hydrometeorol.*,
863 10(4), 1011–1025, doi:10.1175/2008jhm1067.1, 2009.
- 864 Bogan, T., Mohseni, O. and Stefan, H. G.: Stream temperature-equilibrium temperature
865 relationship, *Water Resour. Res.*, 39(9), doi:1245 10.1029/2003wr002034, 2003.
- 866 Bondeau, A., Smith, P. C., Zaehle, S., Schaphoff, S., Lucht, W., Cramer, W., Gerten, D., Lotze-
867 Campen, H., Müller, C., Reichstein, M. and Smith, B.: Modelling the role of agriculture for the
868 20th century global terrestrial carbon balance, *Glob. Change Biol.*, 13(3), 679–706,
869 doi:10.1111/j.1365-2486.2006.01305.x, 2007.
- 870 Brienen, R. J. W., Phillips, O. L., Feldpausch, T. R., Gloor, E., Baker, T. R., Lloyd, J., Lopez-
871 Gonzalez, G., Monteagudo-Mendoza, A., Malhi, Y., Lewis, S. L., Vásquez Martinez, R.,
872 Alexiades, M., Álvarez Dávila, E., Alvarez-Loayza, P., Andrade, A., Aragão, L. E. O. C.,
873 Araujo-Murakami, A., Arends, E. J. M. M., Arroyo, L., Aymard C., G. A., Bánki, O. S., Baraloto,
874 C., Barroso, J., Bonal, D., Boot, R. G. A., Camargo, J. L. C., Castilho, C. V., Chama, V., Chao,
875 K. J., Chave, J., Comiskey, J. A., Cornejo Valverde, F., da Costa, L., de Oliveira, E. A., Di Fiore,
876 A., Erwin, T. L., Fauset, S., Forsthofer, M., Galbraith, D. R., Grahame, E. S., Groot, N., Hérault,
877 B., Higuchi, N., Honorio Coronado, E. N., Keeling, H., Killeen, T. J., Laurance, W. F., Laurance,
878 S., Licona, J., Magnussen, W. E., Marimon, B. S., Marimon-Junior, B. H., Mendoza, C., Neill,
879 D. A., Nogueira, E. M., Núñez, P., Pallqui Camacho, N. C., Parada, A., Pardo-Molina, G.,
880 Peacock, J., Peña-Claros, M., Pickavance, G. C., Pitman, N. C. A., Poorter, L., Prieto, A.,
881 Quesada, C. A., Ramírez, F., Ramírez-Angulo, H., Restrepo, Z., Roopsind, A., Rudas, A.,
882 Salomão, R. P., Schwarz, M., Silva, N., Silva-Espejo, J. E., Silveira, M., Stropp, J., Talbot, J., ter
883 Steege, H., Teran-Aguilar, J., Terborgh, J., Thomas-Caesar, R., Toledo, M., Torello-Raventos,
884 M., Umetsu, R. K., van der Heijden, G. M. F., van der Hout, P., Guimarães Vieira, I. C., Vieira,
885 S. A., Vilanova, E., Vos, V. A. and Zagt, R. J.: Long-term decline of the Amazon carbon sink,
886 *Nature*, 519(7543), 344–348, doi:10.1038/nature14283, 2015.
- 887 Bustillo, V., Victoria, R. L., de Moura, J. M. S., Victoria, D. D., Andrade Toledo, A. M. and
888 Colicchio, E.: Biogeochemistry of carbon in the Amazonian floodplains over a 2000-km reach:
889 Insights from a process-Based model, *Earth Interact.*, 15(4), 1–29, doi:10.1175/2010EI338.1,
890 2011.
- 891 Coe, M. T., Latrubblesse, E. M., Ferreira, M. E. and Amsler, M. L.: The effects of deforestation
892 and climate variability on the streamflow of the Araguaia River, Brazil, *Biogeochemistry*, 105(1-
893 3), 119–131, doi:10.1007/s10533-011-9582-2, 2011.

- 894 Cole, J. J. and Caraco, N. F.: Carbon in catchments: connecting terrestrial carbon losses with
895 aquatic metabolism, *Mar. Freshw. Res.*, 52(1), 101–110, 2001.
- 896 Cole, J. J., Pace, M. L., Carpenter, S. R. and Kitchell, J. F.: Persistence of net heterotrophy in
897 lakes during nutrient addition and food web manipulations, *Limnol. Oceanogr.*, 45(8), 1718–
898 1730, 2000.
- 899 Cole, J. J., Prairie, Y. T., Caraco, N. F., McDowell, W. H., Tranvik, L. J., Striegl, R. G., Duarte,
900 C. M., Kortelainen, P., Downing, J. A., Middelburg, J. J. and Melack, J.: Plumbing the global
901 carbon cycle: Integrating inland waters into the terrestrial carbon budget, *Ecosystems*, 10(1),
902 171–184, doi:10.1007/s10021-006-9013-8, 2007.
- 903 Collatz, G. J., Ribas-Carbo, M. and Berry, J. A.: Coupled photosynthesis-stomatal conductance
904 model for leaves of C4 plants, *Funct. Plant Biol.*, 19(5), 519–538, doi:10.1071/PP9920519, 1992.
- 905 Cooley, S. R. and Yager, P. L.: Physical and biological contributions to the western tropical
906 North Atlantic Ocean carbon sink formed by the Amazon River plume, *J. Geophys. Res.-Oceans*,
907 111(C08018), doi:10.1029/2005JC002954, 2006.
- 908 Cooley, S. R., Coles, V. J., Subramaniam, A. and Yager, P. L.: Seasonal variations in the
909 Amazon plume-related atmospheric carbon sink, *Glob. Biogeochem. Cycles*, 21(3),
910 doi:10.1029/2006GB002831, 2007.
- 911 Cramer, W., Bondeau, A., Woodward, F. I., Prentice, I. C., Betts, R. A., Brovkin, V., Cox, P. M.,
912 Fisher, V., Foley, J. A., Friend, A. D., Kucharik, C., Lomas, M. R., Ramankutty, N., Sitch, S.,
913 Smith, B., White, A. and Young-Molling, C.: Global response of terrestrial ecosystem structure
914 and function to CO₂ and climate change: results from six dynamic global vegetation models,
915 *Glob. Change Biol.*, 7(4), 357–373, 2001.
- 916 Devol, A. H., Quay, P. D., Richey, J. E. and Martinelli, L. A.: The role of gas-exchange in the
917 inorganic carbon, oxygen, and Rn-222 budgets of the Amazon river, *Limnol. Oceanogr.*, 32(1),
918 235–248, 1987.
- 919 Devol, A. H., Forsberg, B. R., Richey, J. E. and Pimentel, T. P.: Seasonal variation in chemical
920 distributions in the Amazon (Solimões) river: A multiyear time series, *Glob. Biogeochem.*
921 Cycles, 9(3), 307–328, 1995.
- 922 Diegues, A. C. S.: An inventory of Brazilian wetlands, *Union Internationale pour la
923 Conservation de la Nature et de ses Ressources*, Switzerland, Gland, Switzerland., 1994.
- 924 Druffel, E. R. M., Bauer, J. E. and Griffin, S.: Input of particulate organic and dissolved
925 inorganic carbon from the Amazon to the Atlantic Ocean, *Geochem. Geophys. Geosystems*, 6,
926 Q03009, doi:10.1029/2004GC000842, 2005.
- 927 Ertel, J. R., Hedges, J. I., Devol, A. H., Richey, J. E. and Ribeiro, M. D. G.: Dissolved humic
928 substances of the Amazon river system, *Limnol. Oceanogr.*, 31(4), 739–754, 1986.

- 929 Fader, M., Rost, S., Müller, C., Bondeau, A. and Gerten, D.: Virtual water content of temperate
930 cereals and maize: Present and potential future patterns, *J. Hydrol.*, 384(3-4), 218–231,
931 doi:10.1016/j.jhydrol.2009.12.011, 2010.
- 932 Farquhar, G. D., van Caemmerer, S. and Berry, J. A.: A biochemical model of photosynthetic
933 CO₂ assimilation in leaves of C3 species, *Planta*, 149, 78–90, 1980.
- 934 Fearnside, P. M.: Are climate change impacts already affecting tropical forest biomass?, *Glob.
935 Environ. Change-Hum. Policy Dimens.*, 14(4), 299–302, doi:10.1016/j.gloenvcha.2004.02.001,
936 2004.
- 937 Furch, K. and Junk, W. J.: The chemical composition, food value, and decomposition of
938 herbaceous plants, leaves, and leaf litter of floodplain forests, in *The Central Amazon
939 Floodplain*, edited by W. J. Junk, pp. 187–205, Springer, Berlin, Germany., 1997.
- 940 Gaillardet, J., Dupré, B., Allègre, C. J. and Négrel, P.: Chemical and physical denudation in the
941 Amazon River basin, *Chem. Geol.*, 142(3-4), 141–173, 1997.
- 942 Gerten, D., Schaphoff, S., Haberlandt, U., Lucht, W. and Sitch, S.: Terrestrial vegetation and
943 water balance - hydrological evaluation of a dynamic global vegetation model, *J. Hydrol.*, 286(1-
944 4), 249–270, doi:10.1016/j.jhydrol.2003.09.029, 2004.
- 945 Gerten, D., Rost, S., von Bloh, W. and Lucht, W.: Causes of change in 20th century global river
946 discharge, *Geophys. Res. Lett.*, 35(20), doi:L20405 10.1029/2008gl035258, 2008.
- 947 Gordon, W. S., Famiglietti, J. S., Fowler, N. L., Kittel, T. G. F. and Hibbard, K. A.: Validation of
948 simulated runoff from six terrestrial ecosystem models: results from VEMAP, *Ecol. Appl.*, 14(2),
949 527–545, doi:10.1890/02-5287, 2004.
- 950 Goulding, M., Barthem, R. and Ferreira, E.: *The Smithsonian Atlas of the Amazon*, Smithsonian,
951 Washington and London., 2003.
- 952 Gumpenberger, M., Vohland, K., Heyder, U., Poulter, B., Macey, K., Rammig, A., Popp, A. and
953 Cramer, W.: Predicting pan-tropical climate change induced forest stock gains and losses—
954 implications for REDD, *Environ. Res. Lett.*, 5(1), 014013, doi:10.1088/1748-9326/5/1/014013,
955 2010.
- 956 Hamilton, S. K., Sippel, S. J., Calheiros, D. F. and Melack, J. M.: An anoxic event and other
957 biogeochemical effects of the Pantanal wetland on the Paraguay River, *Limnol. Oceanogr.*,
958 42(2), 257–272, 1997.
- 959 Hedges, J. I., Cowie, G. L., Richey, J. E., Quay, P. D., Benner, R., Strom, M. and Forsberg, B.
960 R.: Origins and processing of organic matter in the Amazon river as indicated by carbohydrates
961 and amino acids, *Limnol. Oceanogr.*, 39(4), 743–761, 1994.
- 962 Hedges, J. I., Mayorga, E., Tsamakis, E., McClain, M. E., Aufdenkampe, A., Quay, P., Richey, J.
963 E., Benner, R., Opsahl, S., Black, B., Pimentel, T., Quintanilla, J. and Maurice, L.: Organic

- 964 matter in Bolivian tributaries of the Amazon River: A comparison to the lower mainstream,
965 Limnol. Oceanogr., 45(7), 1449–1466, 2000.
- 966 Horn, M. H., Correa, S. B., Parolin, P., Pollux, B. J. A., Anderson, J. T., Lucas, C., Widmann, P.,
967 Tjiu, A., Galetti, M. and Goulding, M.: Seed dispersal by fishes in tropical and temperate fresh
968 waters: The growing evidence, Acta Oecologica, 37, 561–577, doi:10.1016/j.actao.2011.06.004,
969 2011.
- 970 Huntingford, C., Zelazowski, P., Galbraith, D., Mercado, L. M., Sitch, S., Fisher, R., Lomas, M.,
971 Walker, A. P., Jones, C. D., Booth, B. B. B., Malhi, Y., Hemming, D., Kay, G., Good, P., Lewis,
972 S. L., Phillips, O. L., Atkin, O. K., Lloyd, J., Gloor, E., Zaragoza-Castells, J., Meir, P., Betts, R.,
973 Harris, P. P., Nobre, C., Marengo, J. and Cox, P. M.: Simulated resilience of tropical rainforests
974 to CO₂-induced climate change, Nat. Geosci., 6(4), 268–273, doi:10.1038/ngeo1741, 2013.
- 975 Irion, G.: Die Entwicklung des zentral- und oberamazonischen Tieflands im Spät-Pleistozän und
976 im Holozän, Amazoniana, 6(1), 67–79, 1976.
- 977 Irmiger, U.: Litterfall and nitrogen turnover in an Amazonian blackwater inundation forest, Plant
978 Soil, 67(1-3), 355–358, 1982.
- 979 Johnson, M. S., Lehmann, J., Selva, E. C., Abdo, M., Riha, S. and Couto, E. G.: Organic carbon
980 fluxes within and streamwater exports from headwater catchments in the southern Amazon,
981 Hydrol. Process., 20(12), 2599–2614, 2006.
- 982 Junk, W. J.: The Amazon floodplain - A sink or source for organic carbon?, Mitteilungen Geol.-
983 Paläontol. Inst. Univ. Hambg., 58, 267–283, 1985.
- 984 Junk, W. J. and Piedade, M. T. F.: Plant life in the floodplain with special reference to
985 herbaceous plants, in The Central Amazon Floodplain, edited by W. J. Junk, pp. 147–185,
986 Springer, Berlin, Germany., 1997.
- 987 Junk, W. J. and Wantzen, K. M.: The flood pulse concept: New aspects, approaches and
988 applications - An update, in Proceedings of the Second International Symposium on the
989 Management of large Rivers for Fisheries, edited by R. L. Welcomme and T. Petr, pp. 117–140.,
990 2004.
- 991 Jupp, T. E., Cox, P. M., Rammig, A., Thonicke, K., Lucht, W. and Cramer, W.: Development of
992 probability density functions for future South American rainfall, New Phytol., 187, 682–693,
993 doi:10.1111/j.1469-8137.2010.03368.x, 2010.
- 994 Keeling, C. D. and Whorf, T. P.: Atmospheric CO₂ records from sites in the SIO air sampling
995 network, in Trends. A Compendium of Data on Global Change, Carbon Dioxide Inf. Anal. Cent.,
996 Oak Ridge Natl. Lab., US Dep. of Energy, Oak Ridge, Tenn., [online] Available from:
997 <http://cdiac.ornl.gov/trends/co2/sio-keel.html> (Accessed 11 October 2008), 2003.
- 998 Kötzinger, A.: A significant CO₂ sink in the tropical Atlantic Ocean associated with the Amazon
999 River plume, Geophys. Res. Lett., 30(24), doi:10.1029/2003GL018841, 2003.

- 1000 Lampert, W. and Sommer, U.: Limnoökologie, 2. neu bearbeitete Auflage., Thieme, Stuttgart.,
1001 1999.
- 1002 Langerwisch, F., Rost, S., Gerten, D., Poulter, B., Rammig, A. and Cramer, W.: Potential effects
1003 of climate change on inundation patterns in the Amazon Basin, *Hydrol. Earth Syst. Sci.*, 17(6),
1004 2247–2262, doi:10.5194/hess-17-2247-2013, 2013.
- 1005 Lauerwald, R., Laruelle, G. G., Hartmann, J., Ciais, P. and Regnier, P. A. G.: Spatial patterns in
1006 CO₂ evasion from the global river network, *Glob. Biogeochem. Cycles*, 29(5), 534–554,
1007 doi:10.1002/2014GB004941, 2015.
- 1008 Lehner, B. and Döll, P.: Development and validation of a global database of lakes, reservoirs and
1009 wetlands, *J. Hydrol.*, 296(1-4), 1–22, doi:10.1016/j.jhydrol.2004.03.028, 2004.
- 1010 Lewin-Koh, N. J. and Bivand, R.: maptools: Tools for reading and handling spatial objects. R
1011 package version 0.8-7., 2011.
- 1012 Lloyd, J. and Taylor, J. A.: On the temperature-dependence of soil respiration, *Funct. Ecol.*, 8(3),
1013 315–323, 1994.
- 1014 Martius, C.: Decomposition of Wood, in *The Central Amazon Floodplain*, edited by W. J. Junk,
1015 pp. 267–276, Springer, Berlin, Germany., 1997.
- 1016 Mayorga, E., Aufdenkampe, A. K., Masiello, C. A., Krusche, A. V., Hedges, J. I., Quay, P. D.,
1017 Richey, J. E. and Brown, T. A.: Young organic matter as a source of carbon dioxide outgassing
1018 from Amazonian rivers, *Nature*, 436(7050), 538–541, doi:10.1038/nature03880, 2005.
- 1019 McClain, M. E. and Elsenbeer, H.: Terrestrial inputs to Amazon streams and internal
1020 biogeochemical processing, in *The Biogeochemistry of the Amazon Basin*, edited by M. E.
1021 McClain, R. L. Victoria, and J. E. Richey, pp. 185–208, Oxford University Press, New York.,
1022 2001.
- 1023 Meehl, G. A., Stocker, T. F., Collins, W. D., Friedlingstein, P., Gaye, A. T., Gregory, J. M.,
1024 Kitoh, A., Knutti, R., Murphy, J. M., Noda, A., Raper, S. C. B., Watterson, I. G., Weaver, A. J.
1025 and Zhao, Z.-C.: Global climate projections, in *Climate Change 2007: The Physical Science
1026 Basis. Contribution of Working Group I to the Fourth Assessment Report of the
1027 Intergovernmental Panel on Climate Change*, edited by S. Solomon, D. Qin, M. Manning, Z.
1028 Chen, M. Marquis, K. B. Averyt, M. Tignor, and H. L. Miller, Cambridge University Press,
1029 Cambrigde, UK and New York, NY, USA., 2007.
- 1030 Melack, J. M. and Fisher, T. R.: Diel oxygen variations and their ecological implications in
1031 Amazon floodplain lakes, *Arch. Fuer Hydrobiol.*, 98(4), 422–442, 1983.
- 1032 Melack, J. M. and Forsberg, B.: Biogeochemistry of Amazon floodplain lakes and associated
1033 wetlands, in *The Biogeochemistry of the Amazon Basin and its Role in a Changing World*, pp.
1034 235–276, Oxford University Press, Eds. McClain, M. E.; Victoria, R. L.; Richey, J. E., 2001.

- 1035 Melack, J. M., Hess, L. L., Gastil, M., Forsberg, B. R., Hamilton, S. K., Lima, I. B. T. and Novo,
1036 E. M. L. : Regionalization of methane emissions in the Amazon Basin with microwave remote
1037 sensing, *Glob. Change Biol.*, 10(5), 530–544, doi:10.1111/j.1529-8817.2003.00763.x, 2004.
- 1038 Melack, J. M., Novo, E. M. L. M., Forsberg, B. R., Piedade, M. T. F. and L., M.: Floodplain
1039 ecosystem processes, in *Amazonia and Global Change*, edited by M. Keller, M. Bustamante, J.
1040 Gash, and P. Silva Dias, pp. 525–541, American Geophysical Union, Washington, DC., 2009.
- 1041 Mitchell, T. D. and Jones, P. D.: An improved method of constructing a database of monthly
1042 climate observations and associated high-resolution grids, *Int. J. Climatol.*, 25(6), 693–712,
1043 doi:10.1002/joc.1181, 2005.
- 1044 Moreira-Turcq, P., Seyler, P., Guyot, J. L. and Etcheber, H.: Exportation of organic carbon from
1045 the Amazon River and its main tributaries, *Hydrol. Process.*, 17(7), 1329–1344,
1046 doi:10.1002/hyp.1287, 2003.
- 1047 Müller-Hohenstein, K.: Die Tropenzone, in *Die Landschaftsgürtel der Erde*, pp. 51–96, B. G.
1048 Teubner, Stuttgart., 1981.
- 1049 Nakićenović, N., Davidson, O., Davis, G., Grübler, A., Kram, T., Lebre La Rovere, E., Metz, B.,
1050 Morita, T., Pepper, W., Pitcher, H., Sankovski, A., Shukla, P., Swart, R. and Dadi, Z.: IPCC
1051 Special report on emission scenarios, [online] Available from:
1052 <http://www.ipcc.ch/ipccreports/sres/emission/index.php?idp=0>, 2000.
- 1053 Nepstad, D. C., Tohver, I. M., Ray, D., Moutinho, P. and Cardinot, G.: Mortality of large trees
1054 and lianas following experimental drought in an Amazon forest, *Ecology*, 88(9), 2259–2269,
1055 doi:10.1890/06-1046.1, 2007.
- 1056 Neu, V., Neill, C. and Krusche, A. V.: Gaseous and fluvial carbon export from an Amazon forest
1057 watershed, *Biogeochemistry*, 105, 133–147, doi:10.1007/s10533-011-9581-3, 2011.
- 1058 Oksanen, J., Blanchet, F. G., Kindt, R., Legendre, P., O'Hara, R. B., Simpson, G. L., Solymos,
1059 P., Stevens, M. H. H. and Wagner, H.: vegan: Community Ecolgy Package. R package version
1060 1.17.11. [online] Available from: <http://CRAN.R-project.org/package=vegan>, 2011.
- 1061 Österle, H., Gerstengarbe, F. W. and Werner, P. C.: Homogenisierung und Aktualisierung des
1062 Klimadatensatzes des Climate Research Unit der Universitaet of East Anglia, Norwich. 6.
1063 Deutsche Klimatagung 2003 Potsdam, Germany, *Terra Nostra*, 2003(6), 326–329, 2003.
- 1064 Panday, P. K., Coe, M. T., Macedo, M. N., Lefebvre, P. and Castanho, A. D. de A.:
1065 Deforestation offsets water balance changes due to climate variability in the Xingu River in
1066 eastern Amazonia, *J. Hydrol.*, 523, 822–829, doi:10.1016/j.jhydrol.2015.02.018, 2015.
- 1067 Parker, A. J.: The Topographic Relative Moisture Index: An approach to soil-moisture
1068 assessment in mountain terrain, *Phys. Geogr.*, 3(2), 160–168, 1982.

- 1069 Poulter, B., Aragão, L., Heyder, U., Gumpenberger, M., Heinke, J., Langerwisch, F., Rammig,
1070 A., Thonicke, K. and Cramer, W.: Net biome production of the Amazon Basin in the 21st
1071 century, *Glob. Change Biol.*, 16(7), 2062–2075, doi:10.1111/j.1365-2486.2009.02064.x, 2009a.
- 1072 Poulter, B., Aragão, L., Heyder, U., Gumpenberger, M., Heinke, J., Langerwisch, F., Rammig,
1073 A., Thonicke, K. and Cramer, W.: Net biome production of the Amazon Basin in the 21st
1074 century: NBP OF THE AMAZON BASIN, *Glob. Change Biol.*, 16(7), 2062–2075,
1075 doi:10.1111/j.1365-2486.2009.02064.x, 2009b.
- 1076 Rammig, A., Jupp, T., Thonicke, K., Tietjen, B., Heinke, J., Ostberg, S., Lucht, W., Cramer, W.
1077 and Cox, P.: Estimating the risk of Amazonian forest dieback, *New Phytol.*, 187(3), 694–706,
1078 doi:10.1111/j.1469-8137.2010.03318.x, 2010.
- 1079 Randall, D. A., Wood, R. A., Bony, S., Colman, R., Fichefet, T., Fyfe, J., Kattsov, V., Pitman,
1080 A., Shukla, J., Srinivasan, J., Stouffer, R. J., Sumi, A. and Taylor, K. E.: Climate models and
1081 their evaluation, in *Climate Change 2007: The Physical Science Basis. Contribution of Working*
1082 *Group I to the Fourth Assessment Report of the Intergovernmental Panel on Climate Change*,
1083 edited by S. Solomon, D. Qin, M. Manning, Z. Chen, M. Marquis, K. B. Averyt, M. Tignor, and
1084 H. L. Miller, Cambridge University Press., 2007.
- 1085 R Development Core Team and contributors worldwide, N. J.: stats: The R Stats Package version
1086 2.13.0., 2011.
- 1087 Richey, J. E. and Victoria, R. L.: C, N, and P export dynamics in the Amazon river, in
1088 *Interactions of C, N, P and S Biogeochemical Cycles and Global Change*, vol. Vol. 14, Springer
1089 Berlin Heidelberg, Berlin, Heidelberg. [online] Available from: <http://nbn-resolving.de/urn:nbn:de:1111-20111152598> (Accessed 4 April 2014), 1993.
- 1091 Richey, J. E., Hedges, J. I., Devol, A. H., Quay, P. D., Victoria, R., Martinelli, L. and Forsberg,
1092 B. R.: Biogeochemistry of carbon in the Amazon River, *Limnol. Oceanogr.*, 35(2), 352–371,
1093 1990.
- 1094 Richey, J. E., Melack, J. M., Aufdenkampe, A. K., Ballester, V. M. and Hess, L. L.: Outgassing
1095 from Amazonian rivers and wetlands as a large tropical source of atmospheric CO₂, *Nature*,
1096 416(6881), 617–620, doi:10.1038/416617a, 2002.
- 1097 Rost, S., Gerten, D., Bondeau, A., Lucht, W., Rohwer, J. and Schaphoff, S.: Agricultural green
1098 and blue water consumption and its influence on the global water system, *Water Resour. Res.*,
1099 44(9), doi:W09405 10.1029/2007wr006331, 2008.
- 1100 Sander, R.: Compilation of Henry's law constants for inorganic and organic species of potential
1101 importance in environmental chemistry, Air Chemistry Department, Max-Planck Institute of
1102 Chemistry. [online] Available from: <http://www.mpch-mainz.mpg.de/~sander/res/henry.html>,
1103 1999.
- 1104 Schwoerbel, J. and Brendelberger, H.: *Einführung in die Limnologie*, 9. Auflage., Elsevier,
1105 Spektrum Akademischer Verlag, Heidelberg., 2005.

- 1106 Sioli, H.: Sedimentation im Amazonasgebiet, *Int. J. Earth Sci.*, 45(3), 608–633, 1957.
- 1107 Sitch, S., Smith, B., Prentice, I. C., Arneth, A., Bondeau, A., Cramer, W., Kaplan, J. O., Levis,
1108 S., Lucht, W., Sykes, M. T., Thonicke, K. and Venevsky, S.: Evaluation of ecosystem dynamics,
1109 plant geography and terrestrial carbon cycling in the LPJ dynamic global vegetation model,
1110 *Glob. Change Biol.*, 9(2), 161–185, doi:10.1046/j.1365-2486.2003.00569.x, 2003.
- 1111 Sjögersten, S., Black, C. R., Evers, S., Hoyos-Santillan, J., Wright, E. L. and Turner, B. L.:
1112 Tropical wetlands: A missing link in the global carbon cycle?: Carbon cycling in tropical
1113 wetlands, *Glob. Biogeochem. Cycles*, 28, 1371–1386, doi:10.1002/2014GB004844, 2014.
- 1114 Subramaniam, A., Yager, P. L., Carpenter, E. J., Mahaffey, C., Bjorkman, K., Cooley, S.,
1115 Kustka, A. B., Montoya, J. P., Sanudo-Wilhelmy, S. A., Shipe, R. and Capone, D. G.: Amazon
1116 River enhances diazotrophy and carbon sequestration in the tropical North Atlantic Ocean, *Proc.
1117 Natl. Acad. Sci.*, 105(30), 10460–10465, doi:10.1073/pnas.0710279105, 2008.
- 1118 Thonicke, K., Spessa, A., Prentice, I. C., Harrison, S. P., Dong, L. and Carmona-Moreno, C.:
1119 The influence of vegetation, fire spread and fire behaviour on biomass burning and trace gas
1120 emissions: results from a process-based model, *Biogeosciences*, 7(6), 1991–2011,
1121 doi:10.5194/bg-7-1991-2010, 2010.
- 1122 Vannote, R. L., Minshall, G. W., Cummins, K. W., Sedell, J. R. and Cushing, C. E.: River
1123 Continuum Concept, *Can. J. Fish. Aquat. Sci.*, 37(1), 130–137, 1980.
- 1124 Wagner, W., Scipal, K., Pathe, C., Gerten, D., Lucht, W. and Rudolf, B.: Evaluation of the
1125 agreement between the first global remotely sensed soil moisture data with model and
1126 precipitation data, *J. Geophys. Res.*, 108(4611), doi:10.1029/2003JD003663, 2003.
- 1127 Wantzen, K. M., Yule, C. M., Mathooko, J. M. and Pringle, C. M.: Organic matter processing in
1128 tropical streams, in *Aquatic Ecosystems: Tropical Stream Ecology*, pp. 43–64, Elsevier Science
1129 (USA), London., 2008.
- 1130 Waterloo, M. J., Oliveira, S. M., Drucker, D. P., Nobre, A. D., Cuartas, L. A., Hodnett, M. G.,
1131 Langedijk, I., Jans, W. W. P., Tomasella, J., de Araújo, A. C., Pimentel, T. P. and Estrada, J. C.
1132 M.: Export of organic carbon in run-off from an Amazonian rainforest blackwater catchment,
1133 *Hydrol. Process.*, 20(12), 2581–2597, 2006.
- 1134 Worbes, M.: The forest ecosystem of the floodplains, in *The Central Amazon Floodplain*, edited
1135 by W. J. Junk, pp. 223–265, Springer, Berlin, Germany., 1997.
- 1136 WWF HydroSHEDS: HydroSHEDS, [online] Available from: <http://hydrosheds.cr.usgs.gov/>
1137 (Accessed 15 October 2007), 2007.
- 1138 Yarnell, S. M., Mount, J. F. and Larsen, E. W.: The influence of relative sediment supply on
1139 riverine habitat heterogeneity, *Geomorphology*, 80(3-4), 310–324,
1140 doi:10.1016/j.geomorph.2006.03.005, 2006.

1141 Zulkafli, Z., Buytaert, W., Manz, B., Rosas, C. V., Willems, P., Lavado-Casimiro, W., Guyot, J.-
1142 L. and Santini, W.: Projected increases in the annual flood pulse of the Western Amazon,
1143 Environ. Res. Lett., 11(1), 014013, doi:10.1088/1748-9326/11/1/014013, 2016.

1144

1145

1146 7 Tables

1147

1148 Table 1: Overview of the input used in the model.

<i>input</i>	<i>temporal resolution</i>	<i>spatial resolution (lat/lon)</i>	<i>unit</i>	<i>source</i>
static				
<i>river type</i>	-	$0.5^\circ \times 0.5^\circ$	-	(Diegues, 1994; Irion, 1976; Sioli, 1957)
<i>river order</i>	-	$0.5^\circ \times 0.5^\circ$	-	
max. floodable area (<i>MaxInunArea</i>)	-	$0.5^\circ \times 0.5^\circ$	km^2	(Langerwisch et al., 2013)
<i>rout cell</i>	-	$0.5^\circ \times 0.5^\circ$	-	(Rost et al., 2008)
flow velocity (<i>v</i>)	-	$0.5^\circ \times 0.5^\circ$	m s^{-1}	(Langerwisch et al., 2013)
soil depth (<i>soildepth₁</i> , <i>soildepth₂</i>)	-	$0.5^\circ \times 0.5^\circ$		LPJmL
dynamic				
atmospheric CO ₂ (<i>atmCO₂</i>)	annually	globally	ppm	SRES (see Nakićenović et al., 2000)
Temperature (<i>T</i>)	monthly	$0.5^\circ \times 0.5^\circ$	°C	IPCC (see Meehl et al., 2007)
Discharge (<i>Mdis</i>)	monthly	$0.5^\circ \times 0.5^\circ$	$\text{m}^3 \text{s}^{-1}$	LPJmL
amount of water (<i>Mwat</i>)	monthly	$0.5^\circ \times 0.5^\circ$	m^3	LPJmL
soil water content (<i>Mswc₁</i> , <i>Mswc₂</i>)	monthly	$0.5^\circ \times 0.5^\circ$	%	LPJmL
soil carbon (<i>ASoilc</i>)	annually	$0.5^\circ \times 0.5^\circ$	g m^{-2}	LPJmL
litter carbon (<i>ALitc</i>)	annually	$0.5^\circ \times 0.5^\circ$	g m^{-2}	LPJmL

1149

1150

1151

Table 2 List of physical constants.

<i>constant name</i>	<i>value</i>	<i>unit</i>	<i>source</i>
k_H^θ	1.496323	$\text{g CO}_2 \text{l}^{-1} \text{ atm}^{-1}$	(Sander, 1999)
$dlnkH$	2400	K	(Sander, 1999)
T^θ	298.15	K	(Sander, 1999)
$ctoco2^*$	0.2729	-	

1152 * Ratio of the atomic mass of carbon (12.001 g mol⁻¹) in the CO₂ molecule (44.01 g mol⁻¹).1153 Applied to calculate the outgassed CO₂, since the model calculates the actual flux and pools of
1154 carbon.

1155

1156

Table 3: List of parameters.

<i>parameter name</i>	<i>value</i>	<i>unit</i>	<i>source</i>	<i>original value</i>
loss via terrestrial respiration				
$respi_{litr}$	30	%	LPJmL	
$respi_{soilcfast}$	3	%	LPJmL	
$respi_{soilslow}$	0.1	%	LPJmL	
$respipart_{soilcfast}$	98	%	LPJmL	
$respipart_{soilslow}$	2	%	LPJmL	
mobilization				
$carboncorr$	0.65	month^{-1}	(Worbes, 1997)	0.65 ± 0.15
$mobil_{litr}$	0.7	month^{-1}	(Irmler, 1982)	0.4 ± 0.1
$mobil_{soilc}$	0.05	month^{-1}	(Irmler, 1982)	
$mobil_p$	0.5	-	(Johnson et al., 2006; McClain and Elsenbeer, 2001)	0.5 ± 0.25
decomposition				
$decomp$	0.3	month^{-1}	(Furch and Junk, 1997)	0.3 ± 0.1
$decompcorr$	0.1	month^{-1}	(Furch and Junk, 1997)	0.1 ± 0.01
respiration				
$respi$	0.04	day^{-1}	(Cole et al., 2000)	0.045 ± 0.01
outgassing				
$co2satur$	7.25 to 17.0	-	(Richey et al., 2002)	7.25 to 17.0

1157

1158

Table 4: List of data used for calibration and validation.

	<i>observation</i>	<i>simulated</i>	<i>diff</i>	<i>source</i>
annually outgassed CO₂				
basin wide [10 ¹⁴ g C yr ⁻¹]	4.7	1.28	-73%	(Richey et al., 2002)
in central part ^a [10 ¹⁴ g C yr ⁻¹]	2.1 ± 0.6	0.51	-76%	(Richey et al., 2002)
per km ⁻² [10 ⁸ g C km ⁻² yr ⁻¹]	1.2 ± 0.3	0.21	-82%	(Richey et al., 2002)
	6.4 ± 6.0	0.21	-96.7%	(Abril et al., 2014)
	8.0 ± 1.8	0.21	-97.4%	(Belger et al., 2011)
	60 ± 6.8	0.21	-99.7%	(Neu et al., 2011)
annually exported carbon to Atlantic Ocean (estimated at Obidos) [10¹⁴ g C yr⁻¹]				
TOC ^a	0.36 ± 0.1	0.64	+80%	(Richey et al., 1990), (Moreira-Turcq et al., 2003)
POC	0.12 ± 0.05	0.19	+63%	(Junk, 1985; Moreira-Turcq et al., 2003)
DOC	0.27	0.45	+67%	(Moreira-Turcq et al., 2003)
annually exported carbon from sub-catchments [10¹² g C yr⁻¹]				
POC				
Vargem Grande	6.4	8.3	+30%	(Richey and Victoria, 1993)
Rio Madeira	3.2	7.4	+31%	(Richey and Victoria, 1993)
Óbidos	12.1	19.4	+20%	(Richey and Victoria, 1993)
DOC				
Vargem Grande	4.7	21.0	+347%	(Richey and Victoria, 1993)
Rio Negro	6.6	09.2	+39%	(Richey and Victoria, 1993)
Rio Madeira	2.6	17.5	+573%	(Richey and Victoria, 1993)
Óbidos	18.4	45.1	+91%	(Richey and Victoria, 1993)
carbon concentration [10⁻³ g C l⁻¹]				
TOC ^a	9.85 ± 4.5	#7.46	-24%	(Ertel et al., 1986), (Moreira-Turcq et al., 2003)
POC (average)	1.50 ± 0.5	2.16	+44%	(Moreira-Turcq et al., 2003)
Rio Negro	0.69 ± 0.16	1.85 ± 1.33	+170%	(Moreira-Turcq et al., 2003)
Rio Negro	0.37 ± 0.17	0.16	-58%	(Richey et al., 1990)
Rio Branco	0.71 ± 0.28	2.03 ± 0.67	+190%	(Moreira-Turcq et al., 2003)
Rio Solimões	1.26 ± 0.47	0.66 ± 0.61	-48%	(Moreira-Turcq et al., 2003)
Rio Madeira	1.73 ± 1.8	1.42 ± 1.39	-18%	(Moreira-Turcq et al., 2003)
Rio Madeira	2.87 ± 1.24	1.70	-41%	(Richey et al., 1990)
Rio Japura	1.88 ± 0.39	1.02	-46%	(Richey et al., 1990)
Itapeua	3.21 ± 0.52	1.80	-44%	(Richey et al., 1990)
Óbidos	2.41 ± 0.39	0.13	-87%	(Richey et al., 1990)
DOC (average)	7.35 ± 4.0	5.30	-28%	(Ertel et al., 1986; Hedges et al., 1994; Moreira-Turcq et al., 2003)
Rio Negro	11.61 ± 5.49	2.07 ± 1.42	-82%	(Moreira-Turcq et al., 2003)
Rio Negro	8.43 ± 1.20	0.38	-95%	(Richey et al., 1990)
Rio Branco	2.4	2.25 ± 0.75	-6%	(Moreira-Turcq et al., 2003)
Rio Solimões	4.26 ± 1.67	1.52 ± 1.32	-64%	(Moreira-Turcq et al., 2003)
Rio Madeira	4.31 ± 2.23	7.16 ± 5.49	+66%	(Moreira-Turcq et al., 2003)
Rio Madeira	3.49 ± 1.18	0.40	+88%	(Richey et al., 1990)

Rio Japura	3.46 ± 0.66	2.44	-29%	(Richey et al., 1990)
Itapeua	3.76 ± 0.83	3.82	+2%	(Richey et al., 1990)
Óbidos	4.03 ± 0.70	0.74	-82%	(Richey et al., 1990)
IC (average)	0.95-4.08	1.64	-70-60%	(Neu et al., 2011; Richey et al., 2002)
Vargem Grande	1.12	1.84	+64%	(Devol et al., 1987)
Rio Icá	2.07	1.78	-14%	(Devol et al., 1987)
Rio Juruá	2.71	2.67	-02%	(Devol et al., 1987)
Jutica	1.77	1.72	-03%	(Devol et al., 1987)
Manacapuru	1.79	1.64	-08%	(Devol et al., 1987)
Rio Negro	1.44	1.72	+20%	(Devol et al., 1987)
Rio Madeira	2.34	1.75	-25%	(Devol et al., 1987)
Óbidos	1.98	1.69	-15%	(Devol et al., 1987)
Willmott's Index of Agreement				
calibration data ^a	before calibration	0.870	after calibration	0.893
other data		0.413		0.635
all data		0.427		0.615

1160 Comparison of observed values with results of the simulations using initial parameter setting
 1161 (before calibration) and calibrated parameter setting. Difference (*diff*) is relative difference to
 1162 observation [%]. A Willmott's Index of Agreement of 1.0 indicates full agreement. ^a indicates
 1163 data used for calibration.

1164

1165

1166

Table 5: Location and characteristics of the three subregions.

	<i>North-West corner</i>	<i>South-East corner</i>	<i>area [10³km²]</i>	<i>changes in inundation length*</i>	<i>changes in inundated area*</i>
R1	0.5°S / 78.5°W	7.0°S / 72.0°W	523.03	1 month longer	larger
R2	1.0°S / 70.0°W	5.0°S / 52.0°W	891.32	±½ month shift	heterogeneous
R3	4.5°S / 58.0°W	11.0°S / 52.0°W	523.03	½ shorter	smaller

1167 Regions are also depicted in Fig. 6A. *Changes in inundation compared to the average of 1961-
 1168 1990, as estimated and discussed in Langerwisch et al. (2013).

1169

1170

1171

Table 6: Mean monthly export of carbon during reference and future period.

		outgassed carbon to atmosphere									
		Standard ^a					NoInun ^b		NoRiv ^c		
		sum [10 ¹² g yr ⁻¹]	prop of NPP [%]	SUM [10 ¹² g yr ⁻¹]	terr. [%]	riv. [%]	prop of NPP [%]	sum 100% terr. [10 ¹² g yr ⁻¹]	rel. to SUM [%]	sum 100% terr. [10 ¹² g yr ⁻¹]	rel. to SUM [%]
<i>BASIN WIDE</i>											
reference period											
		54.1	1.0	5271.6	5081.8 (96.4)	189.8 (3.6)	3.5	5097.6	-3.3	5266.8	-0.10
future period											
A1B		49.3	0.75	6469.2	6204.0 (95.9)	265.2 (4.1)	4.0	6258	-3.3	6463.2	-0.10
prop. to ref		(-8.9)		(+22.7)				(+22.8)		(+22.7)	
A2		59.1	0.87	6753.6	6463.2 (95.7)	290.4 (4.3)	4.2	6534.0	-3.2	6748.8	-0.07
prop. to ref		(+9.1)		(+28.1)				(+28.2)		(+28.1)	
B1		56.6	0.90	6380.4	6163.6 (96.1)	248.8 (3.9)	3.9	6172.8	-3.3	6375.6	-0.07
prop. to ref		(+4.6)		(+21.0)				(+21.1)		(+21.1)	
<i>MAIN STEM (R2)</i>											
reference period											
				784.8	745.6 (95.0)	39.2 (5.0)	4.9	753.6	-4.0	780	-0.61
future period											
A1B				925.2	873.4 (94.4)	51.8 (5.6)	5.7	888.0	-3.9	920.4	-0.54
prop. to ref				(+17.8)				(+17.9)		(+17.9)	
A2				960.0	903.4 (94.1)	56.6 (5.9)	6.1	921.6	-3.9	954	-0.54
prop. to ref				(+22.3)				(+22.3)		(+22.2)	
B1				930.0	880.7 (94.7)	49.3 (5.3)	5.6	892.8	-3.9	925.2	-0.53
prop. to ref				(+18.4)				(+18.5)		(+18.5)	

1172

Mean export of carbon in reference period (1971-2000) and future period (2070-2099), averaged over five climate models. Discharged carbon in [10¹² g yr⁻¹], outgassed carbon in [10¹² g month⁻¹] from the forest (terr.) and the river (riv.). List of discharged total organic carbon into the Atlantic Ocean and basin wide monthly outgassed carbon produced via heterotrophic respiration. NPP is net primary production. Proportional differences [%] between reference and future period are in round brackets. Differences in total outgassed carbon between future and

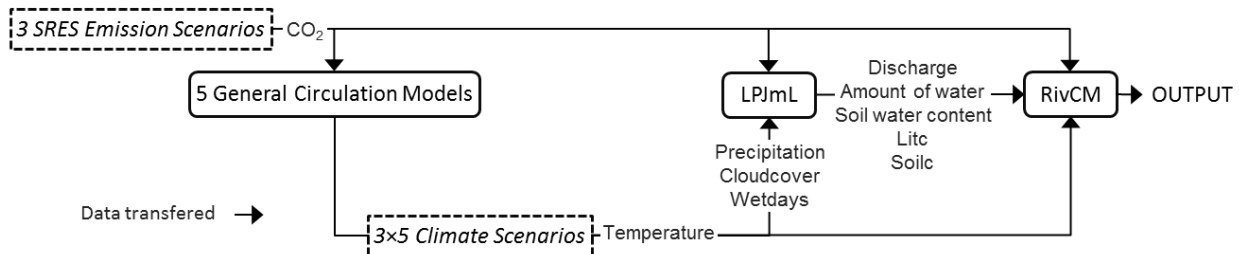
1178 reference values are in all cases highly significant (Wilcoxon Rank-Sum Test; $p<0.001$).
1179 Negative (positive) values indicate a decrease (increase) compared to the *Standard* simulations.
1180 ^a*Standard* RivCM simulations; ^bRivCM simulation without additional inundation (*NoInun*),
1181 therefore no export of terrigenous organic carbon; ^cLPJmL calculating forest instead of river
1182 (*NoRiv*). For details of river area calculation see Langerwisch et al. (2013).

1183

1184

1185 **8 Figures**

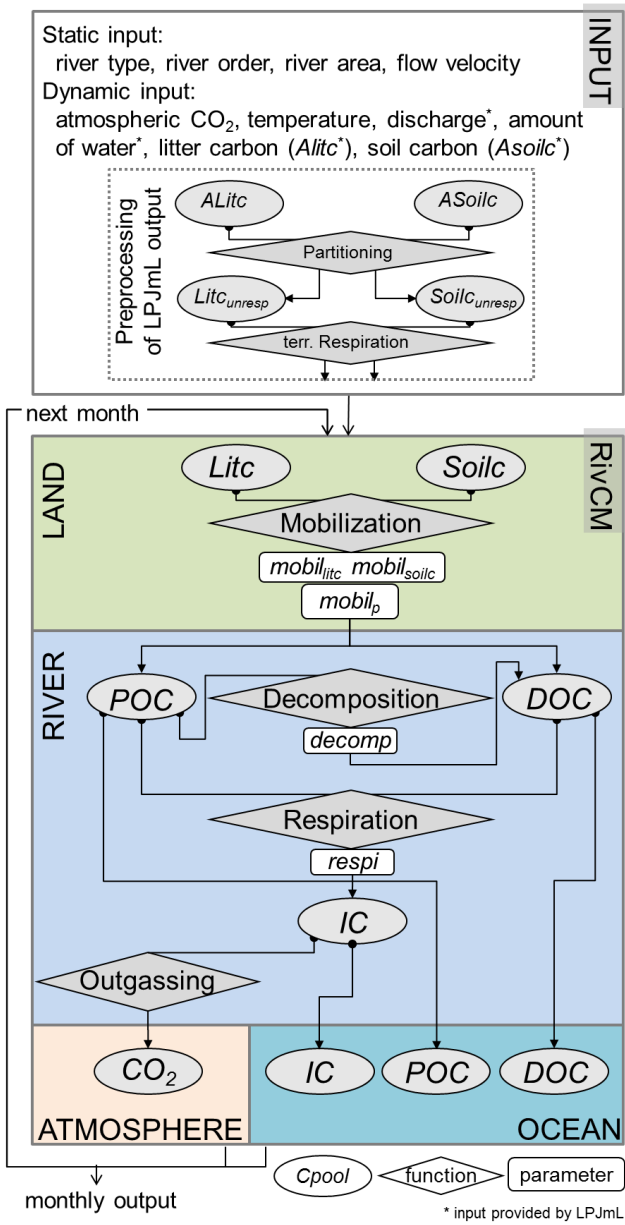
1186



1187

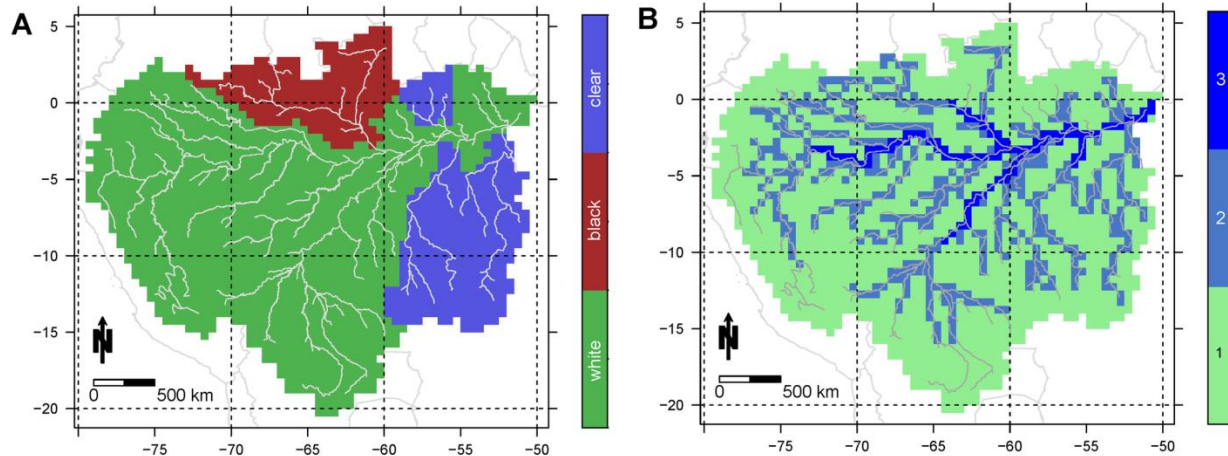
1188 **Figure 1.** Overview about the transfer of data between the models and scenarios.

1189



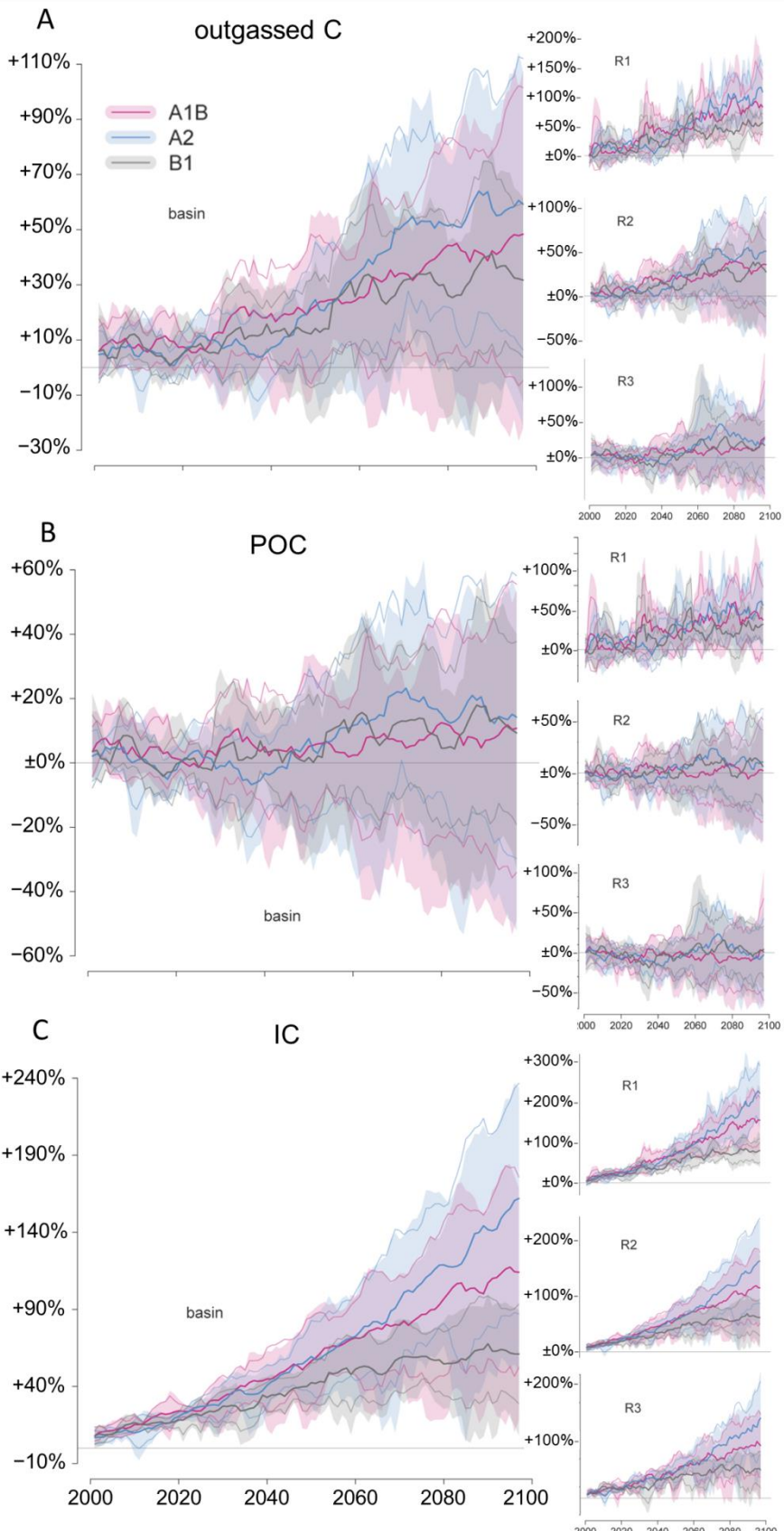
1190

1191 **Figure 2.** Input and flow chart of RivCM. The four spatial components ‘LAND’, ‘RIVER’,
 1192 ‘ATMOSPHERE’, and ‘OCEAN’ are connected by the exchange of carbon between different
 1193 carbon pools (ovals), to, within, and from the river. The carbon pools are transformed through
 1194 the most relevant processes (diamonds) with specific rates and ratios (rectangles). After the
 1195 initialization of the input, calculations are conducted on a monthly basis. Litc = carbon in litter,
 1196 Soilc = carbon in soil, POC = particulate organic carbon, DOC = dissolved organic carbon, IC =
 1197 inorganic carbon.
 1198

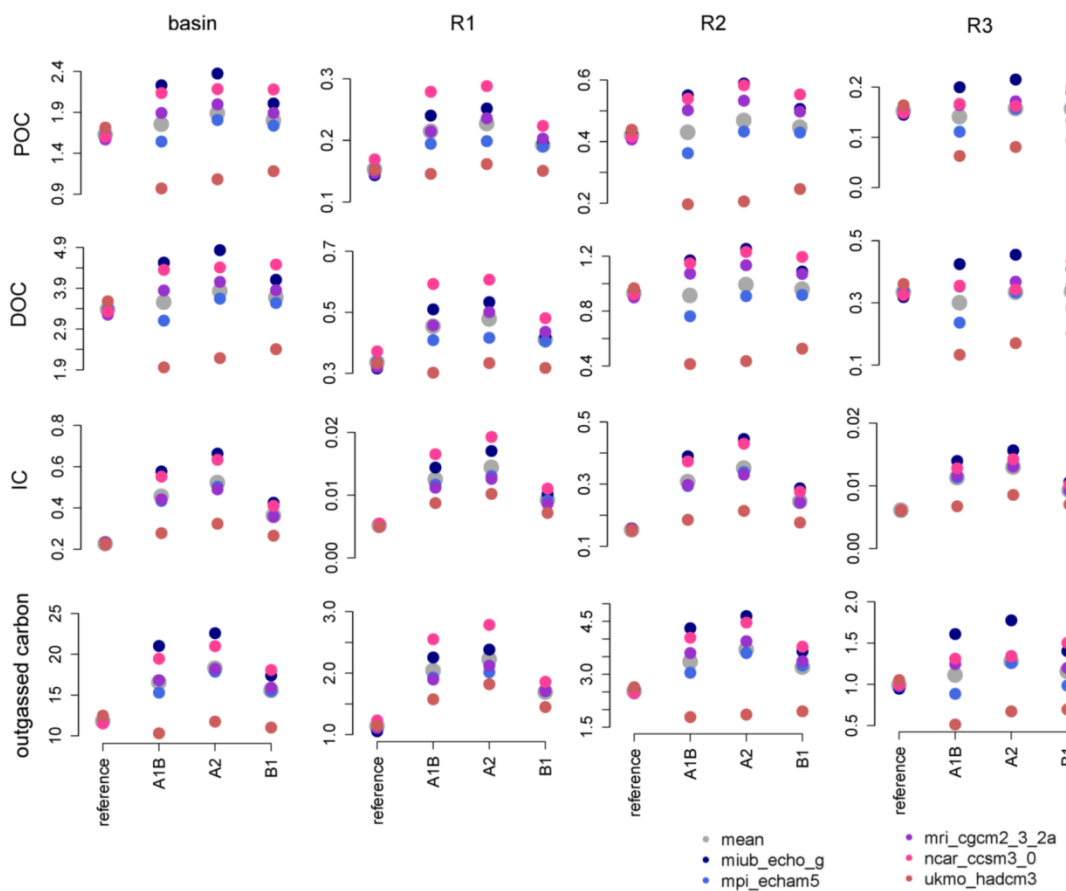


1199

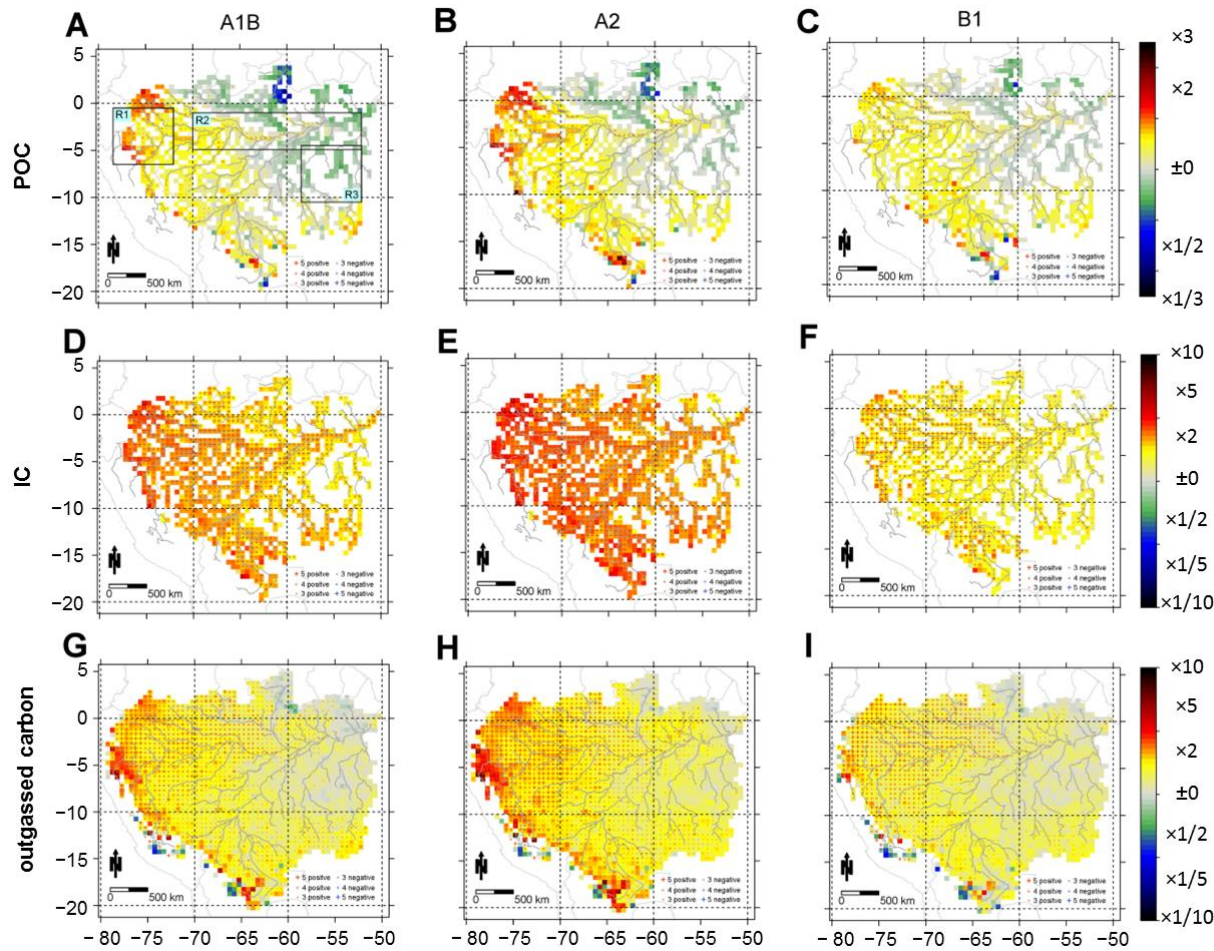
1200 **Figure 3.** River type (A) and river order (B). Cells of river order 1 (headwater)
 1201 have a mean
 1202 annual discharge of less than $8 \times 10^3 \text{ m}^3 \text{ yr}^{-1}$; cells of river order 2 have a discharge between
 1203 8×10^3 and $2 \times 10^5 \text{ m}^3 \text{ yr}^{-1}$; cells of river order 3 have a discharge higher than $2 \times 10^5 \text{ m}^3 \text{ yr}^{-1}$.



1205 **Figure 4.** Temporal change in riverine carbon pools caused by climate change. (A) showing
 1206 results for outgassed carbon, (B) for particulate organic carbon (POC) and (C) for inorganic
 1207 carbon. Results are shown as the quotient of annual carbon amount and mean annual carbon
 1208 amount in reference period, for the whole basin and the three subregions (R1-R3). Different
 1209 colors represent different SRES emission scenarios. The shaded area for each scenario is spanned
 1210 by the minimal and maximal values of all five climate models/scenarios. Bold lines represent the
 1211 5-year-mean of the climate models/scenarios and thin lines represent mean \pm 1.0 standard
 1212 deviation. Positive values indicate an increase in outgassed CO₂ in the future compared to
 1213 reference period, and negative values indicate a decrease. The horizontal line at y = 1 indicates
 1214 no change compared to the reference period 1971-2000.
 1215



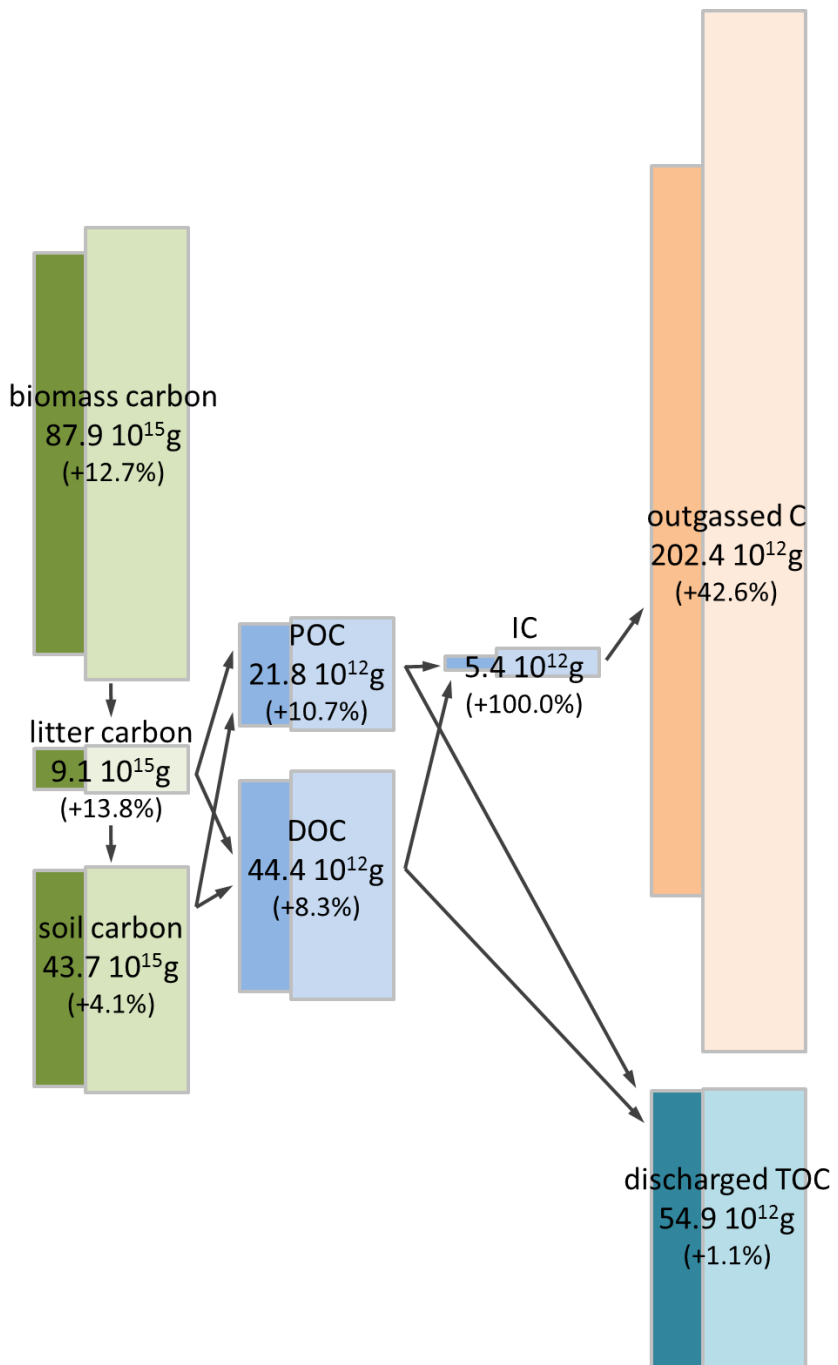
1216
 1217 **Figure 5.** Mean annual sums of carbon pools [10^{12} g] for the whole basin and three subregions
 1218 for the reference period (1971-2000) and the future period (2070-2099, SRES A1B, A2 and B1).
 1219 Each for five climate models/scenarios.
 1220



1221

1222 **Figure 6.** Change in riverine and outgassed carbon caused by climate change. Model mean of the
 1223 relative increase and decrease of future mean and reference mean of POC (A-C) and IC (D-F)
 1224 and outgassed carbon (G-I). Left hand side panels (A, D, G) show the mean of the quotient for
 1225 SRES A1B emission scenario, middle panels (B, E, H) A2, right hand side (C, F, I) B1, averaged
 1226 over five climate models/scenarios. Positive values (yellow and red) indicate an increase and
 1227 negative values (green and blue) indicate a decrease. Additionally to the mean, the number of
 1228 climate models/scenarios leading to significant trends ($p < 0.05$, Wilcoxon Rank-Sum Test) is
 1229 indicated by crosses. In white cells the differences between future and reference values are not
 1230 significant.

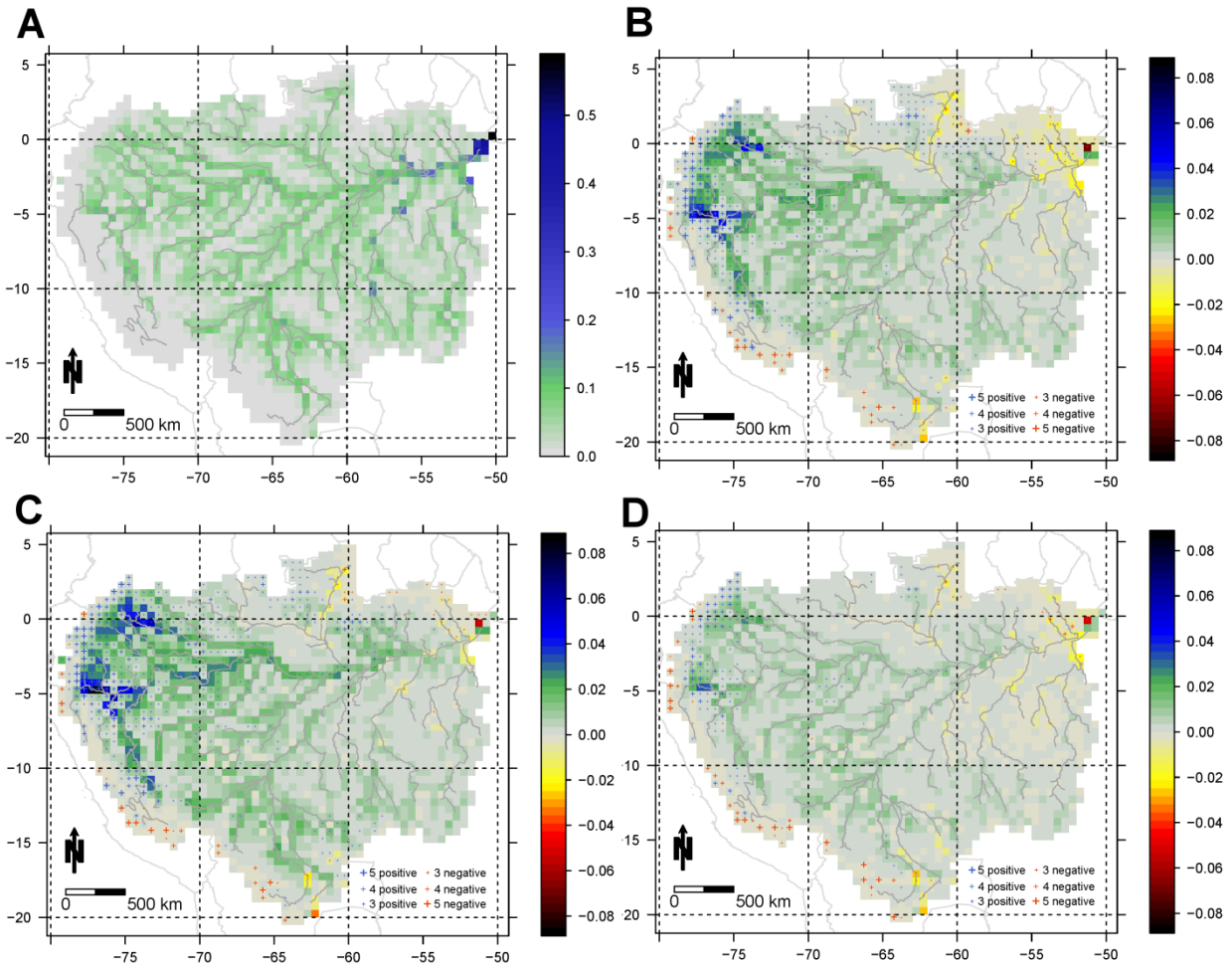
1231



1232

1233 **Figure 7.** Averaged change in the basin carbon budget due to climate change (B). Dark boxes
1234 indicate the amount of carbon during the reference period, light boxes during the future period
1235 (average over all SRES scenarios and GCMs). Amount is given for future period with relative
1236 change compared to reference. Arrows indicate the direction of carbon transport.

1237



1238

1239 **Figure 8.** Proportion of outgassed carbon from the river to total outgassed carbon. Proportion of
1240 riverine outgassing to total outgassing of carbon (A) during the reference period (1971-2000) and
1241 the difference in this proportion between future (2070-2099) and reference period caused by
1242 climate change averaged over five climate models/scenarios in emission scenario A1B (B), A2
1243 (C) and B1 (D), positive values indicate an increase and negative values indicate a decrease in
1244 the future period.

1245